Alfvén Waves in the Solar Atmosphere: From Theory to Observations

Document Version:
Peer reviewed version

Alfvén Waves in the Solar Atmosphere
From Theory to Observations

M. Mathioudakis, D. B. Jess & R. Erdélyi

Abstract Alfvén waves are considered to be viable transporters of the non-thermal energy required to heat the Sun's quiescent atmosphere. An abundance of recent observations, from state-of-the-art facilities, have reported the existence of Alfvén waves in a range of chromospheric and coronal structures. Here, we review the progress made in disentangling the characteristics of transverse kink and torsional linear magnetohydrodynamic (MHD) waves. We outline the simple, yet powerful theory describing their basic properties in (non-)uniform magnetic structures, which closely resemble the building blocks of the real solar atmosphere.

1 Introduction

The solar coronal plasma is an ionized gas which is mainly confined by the ubiquitous presence of magnetic flux tubes and open magnetic field lines. These structures demonstrate sizes over very large scales, right down to the current observational limit, and are maintained at temperatures of several million Kelvin. The heating processes that generate, and sustain the hot corona have so far defied quantitative understanding, despite efforts spanning more than half a century (Kuperus et al. 1981; Gomez 1990; Zirker 1993; Ofman 2005; Klimchuk

M. Mathioudakis & D. B. Jess
Astrophysics Research Center
School of Mathematics and Physics
Queen's University Belfast
Belfast BT7 1NN, Northern Ireland, UK
Tel.: +44 28 9097 3573
Fax: +44 28 9097 3997
E-mail: m.mathioudakis@qub.ac.uk, d.jess@qub.ac.uk

R. Erdélyi
Solar Physics & Space Plasma Research Center (SP^{2}RC)
School of Mathematics and Statistics
University of Sheffield
Sheffield S3 7RH, UK
E-mail: robertus@sheffield.ac.uk

2006; Taroyan & Erdélyi 2009). Efforts to establish the causes of solar atmospheric heating have produced a number of theories, of which two classes are most promising. The first holds for current dissipation, following reconnection events occurring throughout the atmosphere in the form of micro-flare and nano-flare activity (Parker 1988; Priest & Schrijver 1999; Fujimoto et al. 2011). The second class predicts that the heating is driven by magneto-hydrodynamic (MHD) waves (Alfvén 1947; Osterbrock 1961; Ionson 1978; Hollweg 1991), most likely propagating from the lower atmosphere (Roberts 2000). Turbulence can transfer energy from large scales to small scales. There is growing evidence that MHD turbulence and small-scale reconnections are explicitly linked, with current sheets acting as the dissipative structures. Magnetic reconnection is also observed in simulations of MHD turbulence (Matthaeus & Velli 2011; Rappazzo et al. 2008). Two and three dimensional simulations show that magnetic structures tend to self-organize in space and time, creating a number of current sheets at their boundaries. The intermittency of microflares and nanoflares, combined with the small spatial scales over which the energy release occurs, allows us to refer to them collectively as turbulence (Einaudi et al. 1996; Georgoulis et al. 1998).

Kinetic processes and models that are based on wave particle interactions can not explain yet solar phenomena in a global scale, but are clearly applicable to small spatial scales. Kinetic processes and instabilities are highly relevant in models of plasma heating and solar wind acceleration. Hybrid models consider the acceleration of heavy ions by a spectrum of waves in the solar wind as well the influence of the ions on the wave structure and can reproduce the anisotropic velocity distributions of heavy ions (Scudder 1993a,b; Matthaeus & Velli 2011; Ofman & Viñas 2007).

A strongly related, and also unsolved question, involves the generation and acceleration of the solar wind, which often violently interacts with the magnetosphere and Earth's upper atmosphere. Again, there are strong arguments that MHD waves play a key role in contributing to these important questions of space physics (Belcher 1971; Alazraki & Couturier 1971; Gekelman 1999; Tsurutani et al. 1999). The compelling theory of Alfvén waves, which is the basis and starting point of most of the above seminal work, was developed by Hannes Alfvén (Alfvén 1942), for which he received a Nobel Prize in 1970.

Fast and slow mode magneto-acoustic waves cause compression and rarefaction of the plasma as they propagate, with the magnetic and gas pressures acting as the main restoring forces, although kink modes are highly incompressible and the dominating restoring forces are magnetic tension-driven. Alfvén waves are incompressible, with magnetic tension the only restoring force for linear perturbations. If the perturbations are non-linear in nature, magnetic tension is the dominant restoring force. Alfvén waves will cause primarily Doppler shifts, or specific magnetic field perturbations detectable with spectro-polarimetry in selected magnetically sensitive lines. Magneto-acoustic waves can cause both intensity variations and Doppler shifts. If the oscillating structure is spatially unresolved, the above effects will result in a broader line profile.

A study of the dynamic properties of the interplanetary medium, carried out by the Mariner 5 spacecraft in 1967, has shown large-amplitude Alfvén waves in micro-scale structures (Coleman 1967; Unti & Neugebauer 1968). The largest amplitudes were identified in high velocity streams, but were also detected in low velocity regions. It is suggested that these are the remnants of waves generated near the solar surface, and have managed to propagate into the heliosphere without significant damping. The non-detection of appreciable magneto-acoustic wave power would suggest that these waves may have dissipated their energy in the chromosphere and corona (Belcher & Davis 1971). The Mariner observations, combined with the polar observations carried out by Ulysses, allowed a comprehensive view of turbulence in the heliosphere. Measurements of the solar wind parameters in the ecliptic,

have shown that the Alfvénic turbulence observed in high velocity streams, evolves towards a Kolmogorov-type spectrum with velocity shear helping to drive the process. The polar observations reveal a similar evolution but at a lower pace (Bruno & Carbone 2005). These observations have prompted the development of wave-driven models to explain wind acceleration and heating (Velli 2003) (see Ofman (2010) for a recent review).

The motivation for the search for Alfvén waves in the corona can be traced back to Alfvén (1947). Observations of Alfvén waves in the magnetosphere (e.g. Keiling 2009) have prompted the search for the source of these waves in the lower solar atmosphere. With the advent of state-of-the-art instruments on-board satellite missions and ground-based solar telescopes, Alfvén and transversal kink wave modes have started to be studied in the solar photosphere, chromosphere and corona at an unprecedented level of detail (Aschwanden et al. 1999; Nakariakov et al. 1999; Ofman & Wang 2008; McIntosh et al. 2011). The primary objective of this paper is to give an unbiased, but unavoidably personal account of the recent observational reports of Alfvén waves in the solar atmosphere. This work will be underpinned by the linear magneto-hydrodynamic (MHD) theory that describes these waves in (non-)uniform magnetic structures (e.g. slabs and cylinders), which are considered to be simple, yet accurate descriptions of the actual magnetic building blocks of the solar atmosphere. We point out that the accuracy of slabs, cylinders, and pure linear modes in the description of realistic coronal active region loops is often doubted. Improved 3D MHD computational studies of coronal loops, in more realistic bi-polar active region geometries, has been recently performed by McLaughlin & Ofman (2008), Ofman (2009a), Selwa & Ofman (2010), Schmidt & Ofman (2011), and Selwa et al. (2011a,b).

2 The Transition Region and Corona

2.1 Non-thermal Line Broadening

The global torsional oscillation of a coronal loop, with an axis that is not parallel to the line of sight, can produce periodic variations in the observed spectral line widths (McClements et al. 1991; Erdélyi et al. 1998; Zaqarashvili 2003). The first observational efforts to detect Alfvén waves in transition region (TR) and coronal structures dates back to the 1970s, with observations coming from the SKYLAB and SMM missions. Analysis of UV spectra, obtained with the Naval Research Laboratory spectrograph, revealed non-thermal velocities in the range of 10–30 $km\,s^{-1}$ (Doschek et al. 1976; Cheng et al. 1979). The main conclusion from these studies is that, if the excess line broadening is to be attributed to Alfvén waves, these waves cannot account for the heating. McClements et al. (1991) suggested that unambiguous evidence for Alfvén waves in the TR can be provided by tracking coronal loops as they move from disk center to the limb. The non-thermal widths of emission lines from these loops would be expected to increase as a function of distance from disk centre. These line widths should become maximum at the limb, where the magnetic field lines are predominantly perpendicular to the observer's line of sight. Indeed, SUMER observations have shown a centre to limb increase in the non-thermal line widths of upper chromospheric and TR lines, while the excess broadening of coronal lines is only marginal (see e.g. Erdélyi et al. 1998; Banerjee et al. 2007 and references therein). However, chromospheric and transition region lines are known to suffer from opacity effects. Thus, the center-to-limb variation of the line widths can also be attributed to increased opacity broadening towards the limb.

The line broadening could also be due to the effects of bulk outflow motions that cause differential Doppler shifts along the observer's line-of-sight. The height profile of the tem-
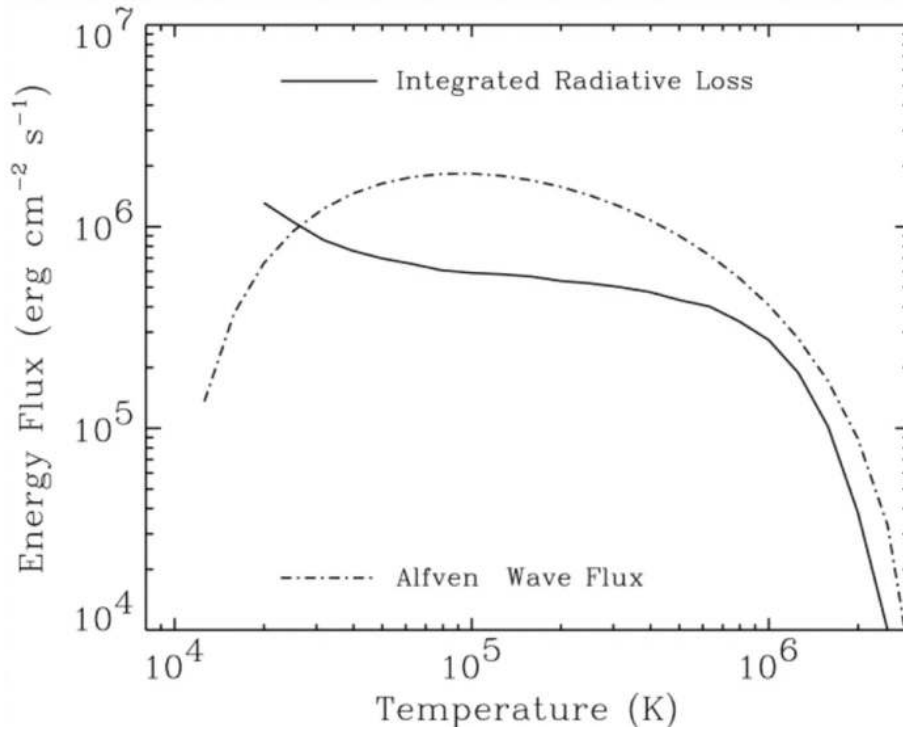
Fig. 1 The Alfvén wave energy flux compared with the radiative losses from the TR and corona (reproduced from Chae et al. 1998).

perature distribution, bulk outflow motions, and the geometry of superradial expansion will enhance the Doppler broadened line profile. These effects are exacerbated by an anisotropic temperature distribution, particularly when $T_{\perp} >> T_{\parallel}$ (Akinari 2007; Ofman 2010a). Raouafi & Solanki (2006) also find that at distances greater that $1R_{\odot}$ from the solar surface, the widths of some transition region and coronal lines depend on the adopted electron density stratification. This became apparent in polar coronal hole observations of O VI and Mg X lines. This may indicate that the need for anisotropic temperature/velocity distributions may not be as important as previously thought.

In a follow up investigation, Chae et al. (1998) argue that the small center-to-limb variation can be due to network cell structures where the non-thermal velocities may be considered isotropic. The authors concluded that if the small increase in the non-thermal velocities of EUV lines is due to Alfvén waves, the limited temporal resolution of the observations would imply that the wave periods will be shorter than a few tens of seconds. They used the non-thermal velocities to derive a wave flux, which was then compared with the radiative losses in the $10^4 - 2\times10^6$ K temperature range. Their comparison reveals that there is sufficient Alfvén wave flux to balance the radiative losses for temperatures in excess of 3×10^4 K. For temperatures lower than 3×10^4 K, the wave energy is significantly smaller than the radiative losses. However, this is inconsistent with Alfvén wave flux which is expected to remain constant (or decrease) as the temperature increases (Chae et al. 1998). This rapid increase in energy as a function of temperature is a direct consequence of the small increase in the non-thermal velocities found in this temperature range (Fig. 1).

2.2 The CoMP View of the Corona

Direct measurements of the coronal magnetic field have been uncertain, and notoriously difficult. Lin et al. (2000) have used the near infrared magnetically sensitive Fe XIII 10747 Å line to measure the Stokes V profiles above active regions, where they determined longitudinal magnetic field strengths in the range of $10 - 33$ G.

The state-of-the-art Coronal Multi-channel Polarimeter (CoMP; Darnell et al. 2003) has been employed behind a coronagraph at the Hill-top facility at the National Solar Observatory in New Mexico, to provide the states of polarization in the 10747 Å line (Tomczyk et al. 2007). The observing setup allows measurements of spectral line intensities, line-of-sight velocities, and line widths in the corona between 1.05 and 1.35 solar radii. The observations show clear evidence for line-of-sight velocity variations with a period of approximately 5 min (3.5 mHz). Simultaneous measurements of linear polarization have revealed the plane-of-the-sky azimuthal component of the coronal magnetic field. Tomczyk et al. (2007) suggested that these oscillations are the signatures of Alfvén waves in the corona for the following reasons: (a) The waves have phase speeds of about 2000 $\mathrm{km\,s^{-1}}$, which is considerably higher than the coronal sound speed, (b) The waves propagate along density structures that are thought to follow the magnetic field lines, and (c) There is no evidence for appreciable intensity oscillations which indicates that the detected wave modes are incompressible. The lack of intensity oscillations may be due to the low spatial resolution that would average out any small scale variations (see later).

The Fourier spectrum of the Doppler velocities associated with these waves points to a photospheric driver (i.e. p-modes). However, since their frequency is below the chromospheric cut-off, the only way that they can propagate upwards into the corona is through inclined magnetic structures (De Pontieu et al. 2004; Erdélyi 2006a,b). They would also need to be converted from pressure-driven modes into non-compressible transversal Alfvén modes.

The interpretation of the CoMP results, in terms of Alfvén waves, has been criticised by e.g. Van Doorsselaere et al. (2008), who argue that these observations show the collective motion of the plasma from its equilibrium position, thus causing a periodic variation in the line-of-sight velocity. The authors suggest the best interpretation is the fast kink mode. We emphasise that even a small intensity perturbation would also point towards the fast kink MHD mode. However, one has to consider how the scales of the photospheric driver compare with the scales of individual threads. If the photospheric driver has dimensions smaller than the threads, the idea of kink waves is favourable. As we are dealing with waves in chromospheric and coronal structures, the kink interpretation becomes more meaningful if the structures are stable over several wave crossing times.

Irrespective of the actual interpretation, there is no doubt that the observational findings of Tomczyk et al. (2007) are sound, and clearly demonstrate the ubiquitous nature of waves in the solar corona. In a follow up investigation, Tomczyk & McIntosh (2009) performed time-distance seismology of the solar corona, and constructed a k–ω diagram of the region. The power spectrum of the coronal velocity perturbations shows an excellent agreement with that of the solar p-modes, which supports the suggestions that these waves can be transported into the corona along inclined flux tubes originating in the photosphere (Fig. 2). However, the high-frequency spectrum is distinctly different from the photospheric power spectrum, and indicates that the high-frequency component of these waves may be generated locally. An estimate of the wave energy reveals that it is significantly smaller than the energy required to balance the coronal radiative losses. However, it should be emphasised that the
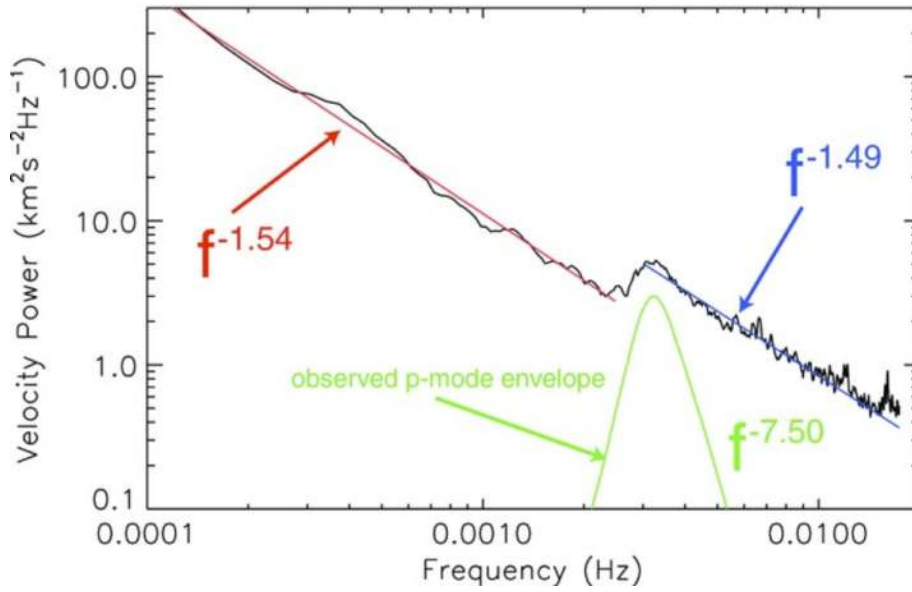
Fig. 2 The Fourier spectrum of the Doppler velocities in the corona (black line) and the photospheric p-mode spectrum (green line). Power-law fits to the low (red) and high frequency (blue) parts of the coronal spectrum are also shown (reproduced from Tomczyk & McIntosh 2009).

low spatial resolution of CoMP, limited to 4.5 arcseconds/pixel, overlooks small-scale solar structures, and therefore significantly underestimates the energy carried by these waves.

The higher spatial resolution of the Atmospheric Imaging Assembly on board the Solar Dynamics Observatory (SDO; Boerner et al. 2011) has indeed shown transverse oscillations in the corona with amplitudes of around 20 km s^{-1}. The amplitude of these motions is a factor of 40 higher that those found by CoMP, and may be sufficiently energetic to balance the radiative losses from the quiet solar corona (McIntosh et al. 2011).

2.3 Flare induced Alfvén Waves

Solar flares often induce temperature rises in the chromosphere of the order of $100 - 200$ K. This requires a significant energy input, amounting to $10 - 20$ erg cm^{-3} s^{-1} at these atmospheric heights. The dense nature of the lower solar atmosphere, when compared to the corona, makes it difficult to reconcile this amount of heating from an individual energy release in the corona (Machado et al. 1978). This is often called the "number problem", whereby the high total number of electrons required to be accelerated down into the lower atmosphere do not exist at coronal heights (Fletcher & Hudson 2008).

An alternative interpretation to explain lower-atmospheric heating is that of flare-induced dissipation of Alfvén waves. Emslie & Sturrock (1982) have suggested how Alfvén-wave perturbations may be generated along current sheets, linking the corona to the lower solar atmosphere, in the aftermath of an impulsive flare event. As the group velocity of Alfvén waves will be parallel to the magnetic field, the energy contained within the mode will remain trapped, providing the wavelength is small compared with the scale length of field and plasma variations. Thus, energy can be readily transported down into the lower solar
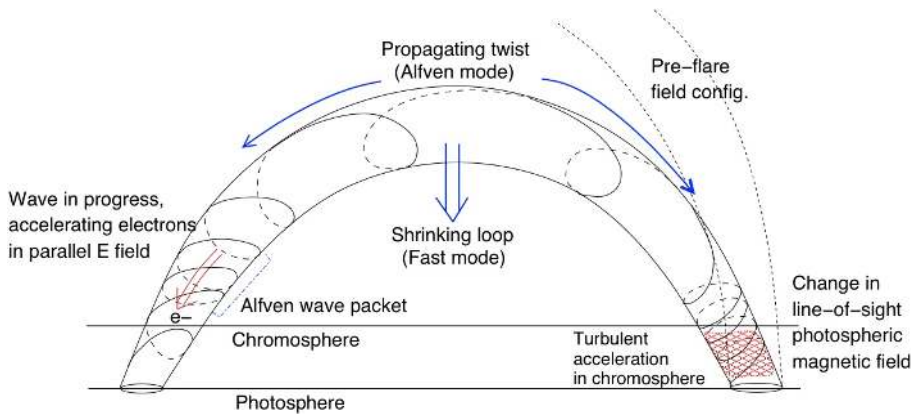
Fig. 3 The coronal magnetic field launches a torsional Alfvén wave pulse into the lower atmosphere, as well as a fast-mode wave pulse. That fraction of the Alfvén wave energy that survives into the chromosphere can also lead to stochastic acceleration there. The wave will be partially reflected from the steep gradients in the chromosphere (not shown) and re-enter the corona (reproduced from Fletcher & Hudson 2008).

atmosphere, where dissipation mechanisms convert the energy into localized heating. The Poynting flux of the waves is proportional to the Alfvén speed and the square of the magnetic field perturbation. X-class flare energy requirements would suggest a Poynting flux of approximately 10^{11} erg cm^{-2} s^{-1}. The magnetic field variations, as high as 200 Gauss (Sudol & Harvey 2005), observed during the most energetic solar flares, combined with the Alfvén speed in the corona, implies that there is sufficient energy to meet the flare requirements (Fletcher & Hudson 2008).

What triggers Alfvén waves during flare events is still an open question. However, current understanding suggests they can be generated during the reconnection process, when the magnetic field relaxes from its stressed pre-flare state (Aulanier et al. 2006). In this regime, magnetic field lines may still be highly distorted from a potential configuration, providing the necessary high-tension force required to induce Alfvén waves (Fig 3; Fletcher & Hudson 2008).

A high degree of Alfvén wave interaction will occur as these waves impact the lower solar atmosphere. Goedbloed & Halberstadt (1994) have shown how incident Alfvén waves will produce a fast-wave spectrum containing rapidly varying amplitudes. It is these waves which can be locally damped through ion-neutral or resistive damping, or form a turbulent cascade which propagates deeper into the photosphere (Emslie & Machado 1979).

Magnetic reconnection can also produce small scale X-ray jets when a burst of solar plasma is driven into the corona at high velocities (Shibata et al. 1992). These X-ray jets, first observed by Yohkoh, have been studied in greater detail by the Hinode X-ray Telescope (XRT). The XRT studies identified a large number of X-ray jets moving with velocities in the range of $200 - 800$ km s^{-1} (Cirtain et al. 2007). The high end of these values is similar to the Alfvén velocity in the corona. The suggestion that an Alfvén wave may be generated in these reconnection sites, prompted Cirtain et al. (2007) to search for transverse oscillations associated with the location of the jets. They identify transverse motions with a period of approximately 200 s, which seem to be related to the high velocity component of the outflow.

3 The Photosphere and Chromosphere

3.1 Transverse Alfvén Waves in Spicules and Fibrils

The wealth of observations from a wide range of ground-based and space-borne missions have shown that the solar chromosphere is permeated by spicules and fibrils. Spicules are dynamic, straw-like magnetic structures that are best identified in the Ca II H & K lines, Na D_3, Hα and Ca II 8542 Å, and can be divided into two distinct classes (Zaqarashvili & Erdélyi 2009). Many detections of transversal waves in spicules have been tied to Type I spicules, which are ubiquitous throughout the solar atmosphere, and longer lived ($\approx$10 min) than their jet-like Type II counterparts (De Pontieu et al. 2007). However, the classification of spicules into two separate types has been recently called into doubt (Zhang et al. 2012). Formed in low plasma β regions, the axis of spicules and fibrils outlines the direction of the magnetic field. Transversal oscillation in these structures, interpreted as Alfvén waves, have recently been reported by De Pontieu et al. (2007). Transverse waves with flows of chromospheric material were also detected in low laying corona loops (Ofman & Wang 2008).These authors used the Solar Optical Telescope (SOT; Tsuneta et al. 2008) on Hinode to analyze a time series of Ca II H (3968 Å) images. The Hinode observations clearly show that spicules undergo transverse motions, with periods in the range of $100 - 500$ s and amplitudes of $10 - 25$ km s^{-1}. The oscillations are evident in traditional $x - t$ plots, where the intensity is plotted as a function of time in a direction perpendicular to the axis of the spicule. The estimated periods can be uncertain as they are comparable to the lifetime of the spicules. Estimates of the energy flux carried by these waves reveals that it is sufficient to balance the radiative losses from the corona and power the solar wind. Recently, He et al. (2009) used a high-cadence mode on Hinode to identify high-frequency oscillations in spicules with periodicities less than 50 s. These waves are interpreted in terms of upwardly propagating Alfvén waves with phase speeds $\geq$75 km s^{-1}, and wavelengths less than 8 Mm (Martinez et al. 2009).

While transverse kink motion has been shown to be abundant in spicule observations, the underlying cause of the periodic motions has remained speculative. Overshooting of convective motions in the photosphere, granular buffeting, rebound shocks, and global p-mode oscillations have all been suggested as candidates for the creation of spicule oscillations (Roberts 1979; Sterling & Hollweg 1988; Vranjes et al. 2008). De Pontieu et al. (2004) have suggested how photospheric p-modes can develop into shocks, and drive the dynamics of chromospheric spicules. The authors indicate how, even though low frequency p-modes become evanescent in the upper photosphere, these waves can propagate upwards into the upper chromosphere and corona through inclined flux tubes. Flux tubes with high inclination angles enhance the leakage of p-modes into the upper layers of the solar atmosphere. Recently, Jess et al. (2012) have presented unambiguous evidence of how the generation of transverse oscillations in spicule structures is a direct result of the mode conversion of longitudinal waves in the lower solar atmosphere. Furthermore, these authors show how spicules are intrinsically linked to photospheric flux concentrations, with their spectrum undoubtedly including signals from both the 3-minute and 5-minute p-mode oscillations (Fig. 4).

The question of how these waves dissipate remains open. Wave energy damping in the inner corona can take place through, e.g. resonant absorption (Ionson 1978; Davila 1987; Hollweg & Yang 1988; Poedts et al. 1989, 1990; Steinolfson & Davila 1993; Ofman et al. 1994, 1995; Ofman & Davila 1995; Erdélyi and Goossens 1995; Ruderman and Roberts 2002; Goossens et al. 2011), phase mixing (Heyvaerts & Priest 1983; Ofman & Aschwanden 2002), Alfvén turbulence (Cranmer & van Ballegooigen 2005; van Ballegooijen et al.
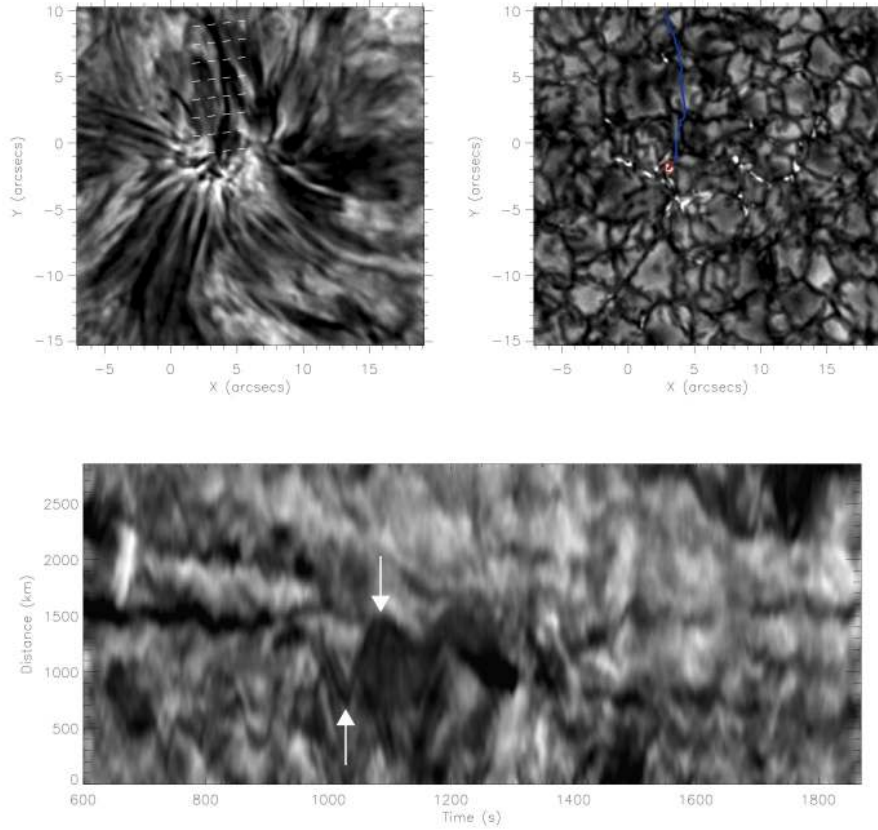
Fig. 4 Simultaneous images of the Hα core (chromosphere; upper left) and G-band (photosphere; upper right), where dashed white lines in the Hα core image highlight the spatial positions where $x - t$ cuts were made. The blue trace in the G-band image denotes the position of a chromospheric spicule (visible in the left panel as a dark, straw-like structure), where one end is anchored into the photosphere above a MBP. A red contour indicates the location where a high concentration of longitudinal oscillatory power is present. The lower panel is a sample Hα time-distance cut, obtained 4000 km (5.5 arcsec) from the underlying MBP, revealing an abundance of periodic transverse motions in the solar chromosphere. White arrows highlight a trough and a peak of a typical transverse oscillation. The scale is in heliocentric coordinates, where 1 arcsec approximately equals 725 km (reproduced from Jess et al. 2012).

2011) and/or mode conversion (Suzuki & Inutsuka 2005). Velli et al. (1989) suggested wave-reflection in the steep density gradients of interplanetary medium as a source of the turbulent cascade of unidirectional Alfvén waves. This idea was applied to the lower solar atmosphere by Matthaeus et al. (1999) who proposed that the Alfvén waves generated in the photosphere and chromosphere interact with their reflections to drive the effects of turbulence offering a viable mechanism for heating the corona in the open field regions. Motivated by the CoMP observations, Verdini et al. (2009) have re-examined the turbulent spectrum from the base of the corona and out to 17 $R_\odot$. They find that turbulent dissipation can account for at least half of the heating required to sustain the solar wind. Reflection driven turbulence can therefore

play a vital role in the acceleration of the fast solar wind. However, the main limitation of these models is the use of incompressible reduced MHD equations. Thus, the likely important coupling between Alfvén waves and compressive modes is neglected in these models. He et al. (2009) suggest that Alfvén waves could instead be damped by cyclotron resonance in the heliosphere, out to 60 $R_{\odot}$, a mechanism that is also favourable for the heating of the solar wind (see reviews by Marsch (2006); Ofman (2010)).

The evolution and dissipation of Alfvénic perturbations in force-free magnetic structures has been studied in detail by Malara et al. (2000), who examined the competing effects of phase mixing and three dimensional effects (i.e. exponential separation of field lines) in wave packet propagation. They find that in a chaotic magnetic field configuration, the dissipation is dominated by three dimensional effects, while in simpler equilibrium situations both phenomena contribute in spatially separated regions. We point out that this approach is limited by the assumption of a incompressibility. Large amplitude Alfvén waves are subject to parametric decay as a result of their coupling with acoustic and transverse waves. The energy of an Alfvén wave propagating in a turbulent medium can be transferred to other wave modes. Malara & Velli (1996) have shown that the parametric instability of non-monochromomatic waves decreases quadratically with departures from the monochromatic case. Numerical simulations of the time evolution of large amplitude Alfvén waves have confirmed the development of this instability in the solar wind (Malara et al. 2000a; Del Zanna et al. 2001).

Spicule oscillations may also be attributed to the transversal kink MHD mode (Zaqarashvili & Erdélyi 2009). The observational signatures of the guided-kink magneto-acoustic mode are the swaying, transversal motions of magnetic flux tubes, similar to the oscillatory behaviour observed in spicules (Erdélyi & Fedun 2007). De Pontieu et al. (2007) have argued that, due to their short lifetime, the spicules cannot act as stable wave guides and the kink mode cannot satisfactory explain the Hinode observations. This apparent contradiction may be resolved by considering the spicule as sliding along the oscillating field lines.

In view of the recent Hinode SOT analysis of spicules, McIntosh et al. (2008) have re-examined the SUMER results of transition region line widths by combining the results of forward modelling with spicule observations. The authors conclude that the C IV intensities and non-thermal velocities can be explained by the superposition of longitudinal mass flows and "Alfvénic motions". It remains unclear what is meant by "Alfvénic motions", since the eigensolutions of MHD equations are not labelled commonly as such in theoretical studies. On the other hand it is not evident that linear MHD eigenmodes of cylindrical magnetic structures can well-describe all realistic coronal conditions. The apparent isotropy in the center-to-limb variations may be explained by the similar magnitude of observed longitudinal and transverse velocity components.

Solar prominences, the heavy and cool elongated magnetic structures supported by mainly horizontal magnetic fields in the solar corona, can support a wide variety of MHD waves. Analysing the properties of these waves can give an unprecedented insight into the small-scale structuring of these features, with clues about the magnetic field strength through means of solar magneto-seismology (Nakariakov & Verwichte 2005).

Prominence oscillations cover a wide range of amplitudes. The large amplitude velocity oscillations, $>20 \ \mathrm{km \ s^{-1}}$, are thought to be excited by Moreton waves produced by flares (Moreton & Ramsey 1960). These oscillations are observed in both the transverse and longitudinal directions, with periods in the range of tens of minutes to a few hours (Tripathi et al. 2009). The potential of large-amplitude prominence oscillations for deriving the vertical magnetic field was first explored by Hyder (1966), who obtained field strengths of tens of Gauss. More recently, Vršnak et al. (2007) used prominence seismology techniques to in-

fer the Alfvén speed, as well as the azimuthal and axial components of the magnetic field strength. The small amplitude oscillations, <3 km s^{-1}, are usually restricted to only part of the prominence, and are thought to be excited by the photospheric and chromospheric oscillations.

The vertical oscillatory motions observed in prominences have been interpreted as transverse waves occurring on the horizontal magnetic field lines of these structures. The oscillations have periods of $2 - 4$ min, and are in phase along the entire length of the prominence thread, as observed in the plane of the sky (Okamoto et al. 2007). The lack of any additional information make the exact wave mode difficult to disentangle. We therefore believe that the suggestion that these oscillations are due to Alfvén waves may be somewhat premature. This is further supported by numerical simulations by e.g. Erdélyi & Fedun (2007). For a recent review on prominence oscillations see Arregui et al. (2012).

3.2 Torsional Alfvén Waves

The periodic motions of photospheric footpoints, in an axially symmetric system, can excite torsional ($m = 0$) Alfvén waves (see §5 of this review and Ruderman et al. 1997; Ruderman 1999). The observational signature of torsional Alfvén waves, with a velocity component along the observers line-of-sight, will arise from torsional velocities on small spatial scales. It is suggested that these torsional velocities will produce an observable full-width half-maximum (FWHM) oscillation in a given line profile. At the linear limit of infinitesimally small amplitude, Alfvén waves are incompressible, and should therefore exhibit no periodic intensity variations.

The detection of such torsional motions in the lower solar atmosphere has, until recently, remained elusive. Jess et al. (2009) used the Swedish Solar Telescope, equipped with the Solar Optical Universal Polarimeter (SOUP; Title 1984), to carry out imaging spectroscopy of the lower solar atmosphere. The tuneable nature of SOUP allowed complete sampling of the Hα profile, and multi-object multi-frame blind deconvolution (van Noort et al. 2005) image reconstruction was implemented to remove small-scale atmospheric fluctuations.

The authors investigated a large conglomeration of photospheric magnetic bright points (MBPs), covering an area of 430,000 km^2. FWHM oscillations of the Hα line profile, in addition to line-of-sight Doppler blue-shift velocities of 23 km s^{-1}, provided evidence for the presence of torsional (m=0) Alfvén waves. The progression of the Doppler-compensated Hα FWHM is shown as a function of time in Figure 5, with a schematic diagram of the observed wave mode shown in Figure 6. A lack of periodic intensity fluctuations in their dataset further strengthened the authors conclusions.

Cauzzi et al. (2009) have used the Interferometric Bi-dimensional Spectrometer (IBIS; Cavallini 2006) to perform imaging spectroscopy of the solar chromospheric network in the Hα and Ca II 8542 Å line. They find that an increased Hα line width correlates well with the Ca II minimum intensity. This is interpreted as evidence for shock heating in the magnetic network which raises the possibility that acoustic shocks can introduce an oscillatory behaviour in the observed Hα line width. To investigate this possibility further, Jess et al. (2009) carried out a number of additional tests to help verify or refute their original conclusions. Since torsional Alfvén waves will produce a FWHM oscillation that is $180°$ out of phase at opposite boundaries of the waveguide (Van Doorsselaere et al. 2008), the authors investigated the instantaneous Hα profile at opposite edges of the MBP group. Through comparison to an at-rest profile, the nature of wing broadening is clearly visible in the lower
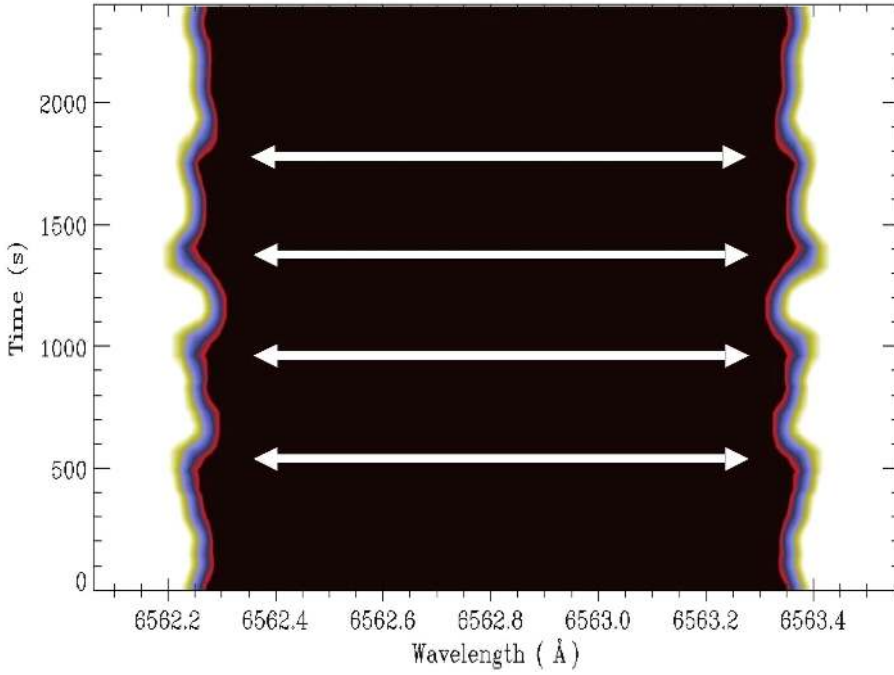
Fig. 5 A wavelength versus time plot of the Hα profile showing the variation of FWHM line width as a function of time. The arrows indicate the positions of maximum amplitude of a 420-s periodicity associated with the MBP group (reproduced from Jess et al. 2009).

panel of Figure 7. These findings reinforce the conclusion of Jess et al. (2009) that the observed FWHM oscillations are due to the presence of torsional Alfvén waves.

The energy flux carried by the Alfvén waves can be estimated using the WKB approximation,

$$F_A = \rho v^2 v_A \ , \tag{1}$$

where ρ is the mass density of the flux-tube, v is the observed velocity amplitude, and v_A the Alfvén speed. For a mass density of $\rho \approx 1 \times 10^{-6}$ kg m^{-3} (Vernazza et al. 1981), and utilizing the derived wave parameters described by Jess et al. (2009), the localised energy flux in the chromosphere is $\approx$150,000 W m^{-2}. It is estimated that, at any given time, $\approx$1.6% of the solar surface is covered by bright point groups (Sánchez Almeida et al. 2010), producing a global average of 2400 W m^{-2}. This value is significantly above the energy required to heat the corona and power the solar wind. We emphasise that the above energy estimate is correct in the absence of vertical gradients or when they can be neglected in the WKB limit. The presence of a soalr wind enhances the transmission of low frequency waves, while high frequency waves have a transmission similar to static models (Heinemann & Olbert 1980; Velli 1993).

4 Wave Drivers

Turbulent convection leads to the stochastic excitation of p-mode oscillations, which are ubiquitous in the lower solar photosphere, and can be detected in both spectral line intensi-
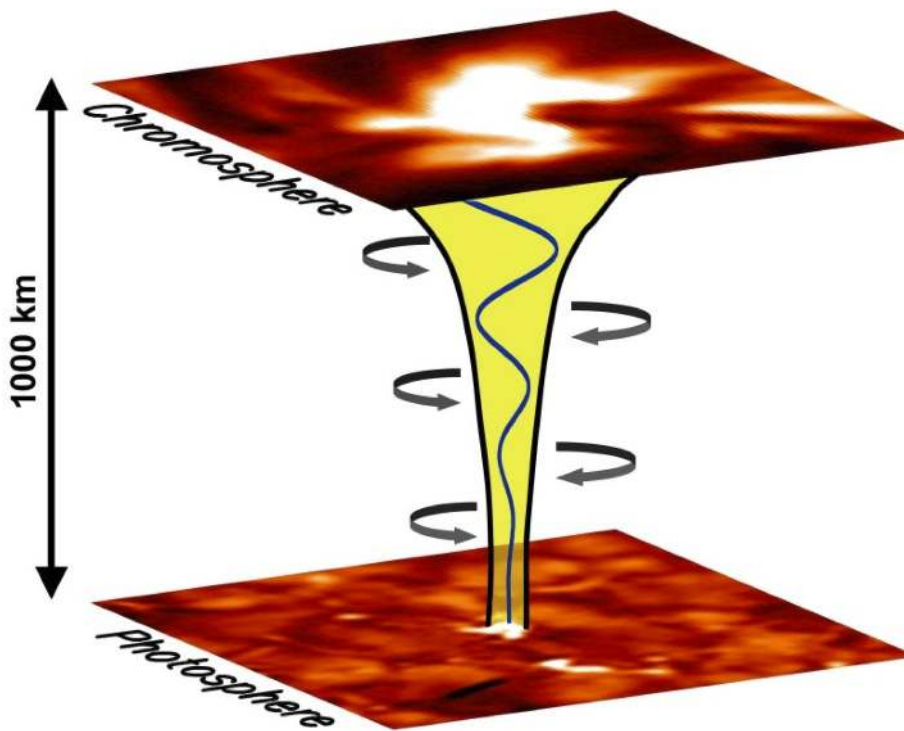
Fig. 6 Schematic diagram of an expanding magnetic flux tube, sandwiched between photospheric and chromospheric intensity images, undergoing a torsional Alfvén perturbation that propagates in the vertical direction. At a given position along the flux tube, the Alfvén displacements are torsional oscillations that remain perpendicular to the direction of propagation (not to scale; reproduced from Jess et al. 2009). A divergent magnetic geometry leads to wave amplitude increase with height and coupling to compressional waves (Ofman & Davila 1998).

ties and Doppler shifts. The frequency of p-mode oscillations are in excess of 1 mHz, with the strongest power detected at $\approx$3 mHz (5 min). However, the p-modes can be modified by the magnetic field (for reviews with references on this subject see e.g. Erdélyi 2006a; Pintér & Erdélyi 2011). In magnetic regions such as sunspots and pores, the amplitudes of the 5-min oscillations are suppressed, while high frequency oscillations, above the acoustic cut-off, have enhanced power. The suppression of low frequency oscillation occurs on very small scales (a few arcseconds), while the enhanced high frequency power occurs primarily in patchy halo-like areas surrounding the strongest magnetic fields (Thomas & Stanchfield 2000).

The solar magnetic network, defined by the boundaries of super-granular flows, shows evidence for MHD waves with frequencies in the range of 1 – 4 mHz. The internetwork has frequencies in excess of 4 mHz, which have been modelled as acoustic waves driven by photospheric velocities (Carlsson & Stein 1997). Network bright points are formed at the boundaries of super-granules, and show a strong correspondence with the underlying magnetic field. The granular buffeting of photospheric flux tubes can create transverse waves which propagate along the field lines and into the upper atmosphere. The models of Musielak & Ulmschneider (2003) suggest that the low frequency oscillations in the magnetic network
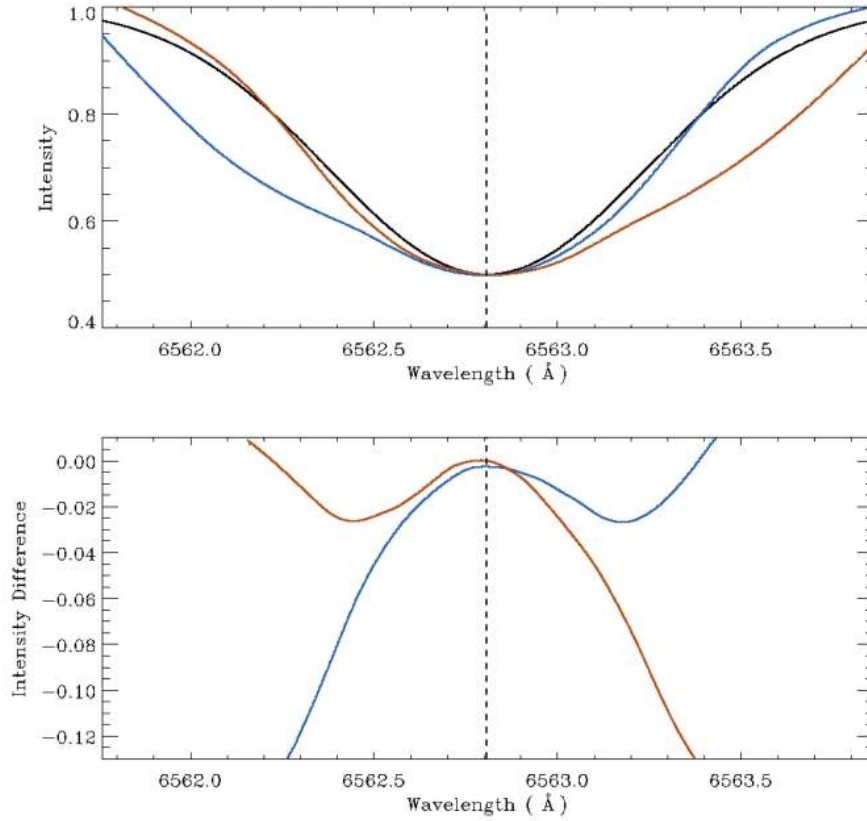
Fig. 7 *Top Panel:* Simultaneous plots of the Hα line profile at opposite edges of the MBP group. The red line shows a profile which is heavily broadened in the red wing of the Hα profile, while the blue line displays a large degree of non-thermal broadening in the blue wing of the Hα profile, at the opposite edge of the MBP group. A rest Hα profile is displayed as a solid black line, with the Hα core rest wavelength plotted as a vertical dashed black line. *Lower Panel:* The same broadened profiles plotted above, but now displayed as intensities relative to the rest Hα profile. It can be seen that the resulting profiles are anti-symmetric about the Hα core rest wavelength of 6562.808Å, as indicated by the vertical dashed black line. This out-of-phase phenomena, at opposite edges of a flux tube undergoing torsional displacements, is a characteristic of the m=0 Alfvén mode.

are due to transverse waves that are generated by the granular buffeting of photospheric flux tubes. Density stratification will lead to an increase in the wave speed as they travel into the upper photosphere and chromosphere, where mode transformation can occur. Transverse waves can transfer power to longitudinal modes, which then develop into shocks and heat the surrounding plasma. A number of criteria may be used to identify if mode transformation has occurred within a given network bright point (Kalkofen 1997; Hasan & Kalkofen 1999; Vigeesh et al. 2011). These include:

– Power at a particular frequency, ν, as identified in the upper-photosphere/lower-chromosphere, should also be identified in the upper chromosphere, but with reduced amplitude.
– Power at double frequency, 2ν, should also appear in the upper chromosphere.

    – Waves remaining at, or above the transverse cut-off, should propagate at approximately the sound speed.

    – The oscillatory signal should be quasi-periodic, as a result of the granular buffeting.

The studies of McAteer et al. (2003) and Bloomfield et al. (2004) have provided the observational evidence for mode coupling in such magnetic networks. In these examples, the authors provide evidence for transverse waves with frequencies in the range 1 – 2.5 mHz, transferring power to longitudinal waves with frequencies of 2 – 5 mHz. We emphasise that the above observational signatures could also appear as a result of nonlinearity.

It has been demonstrated, both analytically and theoretically, that when the magnetic pressure is approximately equal to the gas pressure (plasma $\beta = 1$) in a solar flux tube, longitudinal to transverse mode coupling may also occur (De Moortel et al. 2004). Until recently, this form of "reversed mode coupling" had not been verified observationally. However, Jess et al. (2012) have suggested that longitudinal-to-transverse mode conversion may account for the transversal waves which are ubiquitous in the solar chromosphere. Jess et al. (2012) utilised high spatial and temporal resolution observations, obtained with the Rapid Oscillations in the Solar Atmosphere (ROSA; Jess et al. 2010) imager at the Dunn Solar Telescope, to investigate the origin of transverse oscillations in chromospheric spicules. The authors present strong evidence that transverse oscillations in Type I spicules, with periods in the range of 65 – 220 s, originate in longitudinal oscillations of photospheric magnetic bright points, at twice the transverse period. It must be emphasised that this form of mode coupling occurs in the reverse direction of that reported by McAteer et al. (2003), i.e. longitudinal to transverse. The mechanism for the mode transformation revolves around the nature of the photospheric driver, whereby a $90°$ phase shift across the body of the spicule creates gradients in pressure, which displace the spicule axis, generating the observed kink modes. These periodic pressure differences also induce a frequency doubling of the coupled wave mode, in addition to producing periodic compressions and rarefactions along the body of the spicule (i.e. the sausage mode).

It is known that convective motions, intrinsic to photospheric granulation, transport angular momentum and agitate plasma in the outer layers of the Sun's atmosphere. Solar material rises in the granules and sinks in the inter-granular lanes. The plasma that returns to the solar interior has increased angular momentum, and therefore generates an increased amount of vorticity at the edges of the lanes (Stein & Nordlund 1998). The idea of vortices as the source of torsional wave modes has been proposed by Hollweg et al. (1982) and Velli & Liewer (1999). Small scale vortex motions, with dimensions less than $\approx$500 km, have recently been observed in photospheric G-band images of MBPs (Fig. 8; Bonet et al. 2008). These small scale vortices have lifetimes of a few minutes, and appear to trace the pattern of a super-granular cell. They seem to be formed when two MBPs move towards a common point, and rotate relative to one another. Wedemeyer-Bohm & Rouppe van der Voort (2009) have observed similar vortices in the chromospheric Ca II 8542 Å line core. The location of the chromospheric vortices coincides with photospheric MBPs, although there is no current evidence for simultaneous swirl events in the corresponding photospheric locations.

Recent radiative MHD simulations have shown photospheric vorticities in intergranular magnetic field concentrations (Shelyag et al. 2011). The connection between MBP vortices and upper atmospheric swirls appears to be magnetic in nature. Simulated G-band images show a direct comparison between magnetic vortices and rotary motions of photospheric bright points. These swirly motions of plasma in the intergranular magnetic field concentrations could be responsible for the generation of different types of MHD wave modes such as kink, sausage and torsional Alfvén waves.
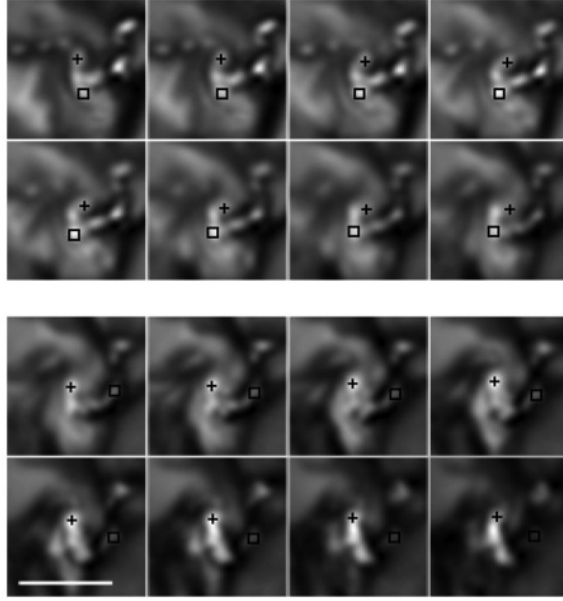
Fig. 8 A sequence of G-band snapshots showing a photospheric vortex. Two pairs of MBPs are marked as squares and crosses to help the reader identify the rotational motions. The snapshots have been taken with a cadence of 15 s. The bar in the lower left corner corresponds to 1,000 km on the solar surface (reproduced from Bonet et al. 2008).

5 Theory

5.1 Alfvén Waves in Uniformly Magnetised Plasma

Within the linear limit of infinitesimally small wave amplitudes in uniform, finite beta magnetized plasma, there are three distinct types of MHD waves that can be mathematically described as: slow and fast magneto-acoustic waves, and Alfvén waves. The first two types of wave have an acoustic character modified by the magnetic field, whereas the Alfvén waves exist purely because of the presence of a magnetic field. The three physically distinct MHD wave modes exist due to the following reasons. The MHD description of a magnetised plasma is using macroscopic quantities, let's say density (ρ), velocity (**v**), magnetic field (**B**) and a thermodynamics variable, say pressure (p). In ideal MHD (i.e. no dissipation or non-adiabatic processes) these quantities are coupled through a set of eight non-linear partial differential equations (PDEs) governing mass conservation, momentum conservation, governing magnetic flux and the energy conservation. If this is a closed system, in a stationary state one may expect eight eigenvalues corresponding to eight different physical wave modes. However, there is the solenoidal condition, that will reduce the number of independent PDEs to seven, resulting in seven eigenvalues. One eigenvalue, $\omega \equiv 0$, turns out to be describing the entropy wave that does not carry information, and may be disregarded, leaving six possible independent eigenvalues corresponding to six further independent modes. An interesting intrinsic feature of the remaining eigenvalues is that they appear squared, i.e.

there is no distinction between forward and backward propagating MHD waves in a *static* (i.e. $\mathbf{v_0} = 0$) magnetised plasma. Hence, there are three physically distinct MHD waves. These waves are a complete set and their appropriate linear superposition can be combined into any linear MHD wave perturbations. This also means that the individual eigenmodes (slow, fast magneto-acoustic and Alfvén waves) are orthogonal to each other and there is no linear transformation that can transform one MHD eigenmode into the other. This latter property is very important when identifying MHD modes in observations. Often, an accurate mode identification is possible only by considering very carefully the mode dispersion or the phase relation between the perturbations involved. An interesting and educational example of this approach is e.g. by Fujimura & Tsuneta (2009). The problem becomes even more subtle in structured plasmas (e.g. magnetic cylinder or slab), where the geometry of the problem introduces an infinite set of MHD eigenmodes.

5.2 Alfvén Waves in Structured, Non-uniform, Magnetised Plasma

A natural way to improve the simplistic view of a uniform MHD plasma (c.f. §5.1), in order to narrow the gap between theory and the observed wave processes taking place in the solar atmosphere, is to add non-uniformity. One way to achieve this goal is to introduce structuring. This may be done in many ways, but both the slab and cylindrical geometry seem to be a popular approach to model the building blocks of the solar atmosphere. We emphasize that the conservation of distinct modes in the real coronal plasma is not guaranteed, since the coronal plasma is nearly always more complex in nature than a collection of slabs and cylinders (Ofman 2009). Another possibility to introduce non-uniformity is to consider inhomogeneity. Inhomogeneity may be either along the waveguide (for example for a vertical magnetic waveguide this could be the gravitational or magnetic stratification) or across (e.g. for a vertical flux tube, this may mean inhomogeneity in the radial direction). It was always expected that once MHD waves are generated, they will easily propagate along magnetic flux tubes (homogeneous or non-uniform), the building block of the solar atmosphere (Fig. 9a), or along magnetic field lines at constant magnetic surfaces (Fig. 9b).

MHD wave theory has been around for a while, in particular for linear magneto-acoustic and Alfvén waves in structured magnetised plasmas (cf., Roberts 1981; Edwin & Roberts 1982 for slab and Edwin & Roberts 1983 for cylindrical geometries). The propagation of torsional Alfvén waves in vertical magnetic tubes have been studied by, e.g., Hollweg (1981); Hollweg et al. (1982) and more recently in the context of filtering torsional Alfvén waves by Fedun et al. (2011b). In order to overview briefly our current understanding of what kind of linear MHD waves are supported by MHD structures, we will assume a simple cylindrical geometry with some non-uniform radial inhomogeneity. We would also point out that it would not be practical to single out the Alfvén wave mode, as there is coupling between the linear MHD modes. The waves have to be investigated in a co-existing context. In nature, however, there may be a physical situation where the excitation mechanism (or driver) would favour one of the modes. Moreover, other wave modes will be produced due to linear (in non-uniform media) and non-linear (even in an initial inhomogeneous plasma) coupling. In order to have the problem tractable for the purpose of wave mode identification, with a focus on Alfvén wave, we assume a uniform magnetic twist here and will follow the key steps of Erdélyi & Fedun (2010).

Let us consider a magnetically twisted straight flux tube embedded within a uniformly magnetised plasma environment in cylindrical geometry. We note, such structures are always unstable, unless they are supported by appropriate boundaries and the twist does not
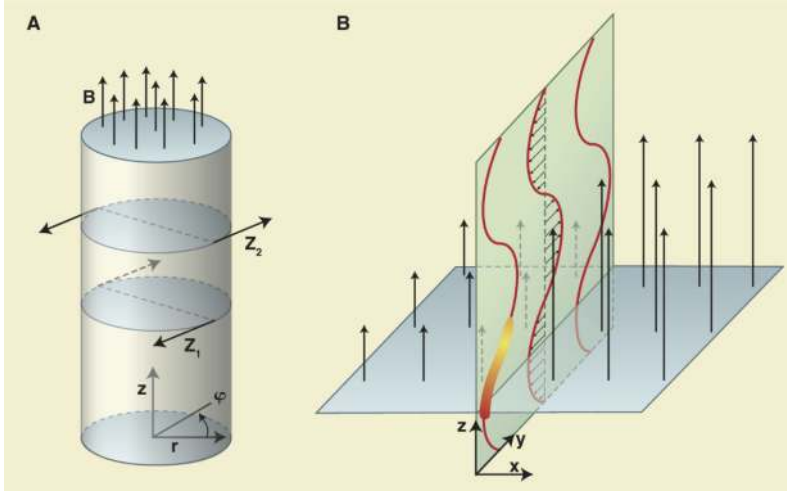
Fig. 9 (A) Magnetic flux tube showing two snapshots (at positions z_1 and z_2) of Alfvén wave perturbations propagating in the longitudinal z direction along field lines. At a given position the Alfvén perturbations are torsional oscillations (i.e. oscillations are in the φ-direction, perpendicular to the background field). (B) Alfvén waves propagating along a constant magnetic surface. The Alfvén perturbations are within the magnetic surface (yz plane) at the discontinuity, perpendicular to the background field (y direction), whereas the waves themselves propagate along the field lines (z direction). Density enhancements (e.g. in the form of spicules as observed by De Pontieu et al. 2007, or within prominences as seen by Okamoto et al. 2007) are visualised here as a yellow-red thin blob that follows the field lines. Vertical arrows indicate the magnetic field gradient increasing from left to right (reproduced from Erdélyi & Fedun 2007).

exceed the critical twist for the MHD kink instability (e.g. Raadu (1972)). The z-axis of the cylindrical coordinate system (r, φ, z) is along the tube. The radius of the tube (r_0) is constant. The unperturbed state and geometry of the model of a magnetically twisted tube is sketched in Figure 10. All dependent variables inside the flux tube have index i, while quantities outside the tube are denoted with index e. In cylindrical equilibrium the magnetic field and plasma pressure satisfy the equilibrium condition in the radial direction:

$$\frac{\mathrm{d}}{\mathrm{d}r}\left(p_{0\mathrm{i}} + \frac{B_{0\mathrm{i}\varphi}^2 + B_{0\mathrm{i}z}^2}{2\mu_0}\right) + \frac{B_{0\mathrm{i}\varphi}^2}{\mu_0 r} = 0. \tag{2}$$

Here, the second term in the brackets represents magnetic pressure and the third term of Equation (2) derives from magnetic tension due to the azimuthal component of the equilibrium magnetic field, $B_{0\mathrm{i}\varphi}$. Gravity is not included in the present analysis. The particular case of a uniformly twisted equilibrium magnetic field, $\mathbf{B_0(r)}$, of the form:

$$\mathbf{B_0(r)} = \begin{cases} (0, Ar, B_{0\mathrm{i}z}), & r \leq r_0, \\ (0, 0, B_{0\mathrm{e}z}), & r > r_0, \end{cases} \tag{3}$$

is considered, where

$$B_{0\mathrm{i}z} = B\left(1 - 2\frac{A^2 r^2}{B^2}\right)^{1/2} \tag{4}$$

in order to satisfy the pressure equilibrium governed by Equation (2). Here A and B are arbitrary constants. This choice of magnetic field may represent solar atmospheric flux tubes with observed weakly twisted field components (see e.g. Klimchuk et al. 2000).
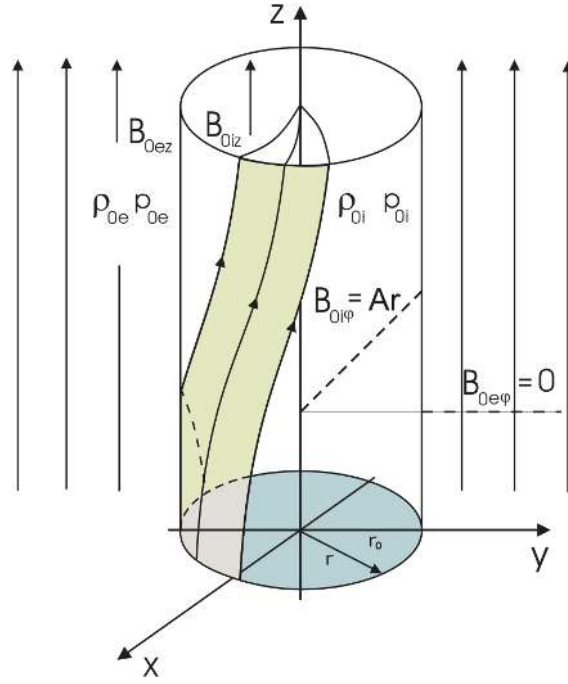
Fig. 10 The equilibrium configuration. The uniformly twisted magnetic flux tube is in an ambient straight and uniform magnetic field. At the boundary of the flux tube there is a jump in magnetic twist (reproduced from Erdélyi & Fedun 2010).

In a cylindrical coordinate system with the equilibrium state inhomogeneous in the radial direction only, $\boldsymbol{\xi} = (\xi_r, \xi_\varphi, \xi_z)$ is the Lagrangian displacement vector denoting perturbations from the equilibrium position; the unperturbed mass density ρ_0 and pressure p_0 are constants (though not equal to zero) inside the flux tube, respectively; $\mathbf{B_0} = (0, B_{0\varphi}(r), B_{0z}(r))$ is the equilibrium magnetic field; μ_0 is the magnetic permeability of free space, p is the perturbation of kinetic plasma pressure and $\mathbf{b}$ is the perturbation of the magnetic field. Let us introduce the Eulerian perturbation of the total pressure: $P_T := p + \mathbf{B_0b}/\mu_0$. Because the equilibrium variables depend on radius only, for normal-mode analysis in cylindrical geometry we Fourier decompose the perturbed variables with respect to φ and z through,

$$\xi, P_T \sim \exp[i(kz + m\varphi - \omega t)] \ .$$

Here ω is the mode frequency, m is the azimuthal order of the mode, k is the longitudinal (axial) wavenumber. Then, after some algebra using the ideal linear MHD equations, one can find that ξ_r and P_T satisfy a system of two first-order ordinary differential equations (see e.g. Appert et al. 1974; Sakurai et al. 1991),

$$D\frac{\mathrm{d}}{\mathrm{d}r}(r\xi_r) = C_1 r\xi_r - rC_2 P_T \ , \text{and} \tag{5}$$

$$D\frac{\mathrm{d}}{\mathrm{d}r}P_T = \frac{1}{r}C_3 r\xi_r - C_1 P_T \ . \tag{6}$$

The choice of variables above does not give much insight into the governing equation of Alfvén waves. We may need to work on further for a more suitable choice of variables,

in order to easier identify perturbations that may be characterised as Alfvén waves. We will do this in due course. Here, the coefficient functions D, C_1, C_2 and C_3 depend on the equilibrium variables and on the frequency ω. In general, these coefficient functions are given as follows:

$$D = \rho_0(\omega^2 - \omega_{\mathrm{A}}^2)C_4, \tag{7}$$

$$C_1 = \frac{2B_{0\varphi}}{\mu_0 r}\left(\omega^4 B_{0\varphi} - \frac{m}{r}f_{\mathrm{B}}C_4\right), \tag{8}$$

$$C_2 = \omega^4 - \left(k^2 + \frac{m^2}{r^2}\right)C_4, \tag{9}$$

$$C_3 = \rho_0 D\left(\omega^2 - \omega_{\mathrm{A}}^2 + \frac{2B_{0\varphi}}{\mu_0\rho_0}\frac{\mathrm{d}}{\mathrm{d}r}\left(\frac{B_{0\varphi}}{r}\right)\right) + 4\omega^4\left(\frac{B_{0\varphi}^2}{\mu_0 r}\right)^2 -$$
$$\rho_0 C_4 \frac{4B_{0\varphi}^2}{\mu_0 r^2}\omega_{\mathrm{A}}^2, \tag{10}$$

where

$$C_4 = \left(C_{\mathrm{S}}^2 + V_{\mathrm{A}}^2\right)\left(\omega^2 - \omega_{\mathrm{C}}^2\right), \tag{11}$$

and

$$C_{\mathrm{S}}^2 = \gamma\frac{p_0}{\rho_0}, \quad V_{\mathrm{A}}^2 = \frac{B_0^2}{\mu_0\rho_0}, \quad B_0^2 = B_{0\varphi}^2 + B_{0z}^2,$$

$$f_{\mathrm{B}} = \frac{m}{r}B_{0\varphi} + kB_{0z}, \quad \omega_{\mathrm{A}}^2 = \frac{f_{\mathrm{B}}^2}{\mu_0\rho_0}, \quad \omega_{\mathrm{C}}^2 = \frac{C_{\mathrm{S}}^2}{C_{\mathrm{S}}^2 + V_{\mathrm{A}}^2}\omega_{\mathrm{A}}^2.$$

Here C_{S} is the sound speed, V_{A} is the Alfvén speed, ω_{A} is the Alfvén frequency and ω_{C} is the cusp frequency. To obtain the remaining perturbed variables, i.e. ξ_φ, ξ_z, b_r, b_φ, b_z and p in terms of ξ_r and P_T we will have

$$\rho_0\omega^2\xi_r = \frac{\mathrm{d}}{\mathrm{d}r}P_T + \frac{2B_{0\varphi}b_\varphi}{\mu_0 r} - \mathrm{i}\frac{f_{\mathrm{B}}b_r}{\mu_0}, \tag{12}$$

$$\rho_0\omega^2\xi_\varphi = \mathrm{i}\frac{m}{r}P_T - \mathrm{i}\frac{f_{\mathrm{B}}b_\varphi}{\mu_0} - \frac{1}{\mu_0}\frac{b_r}{r}\frac{\mathrm{d}}{\mathrm{d}r}\left(rB_{0\varphi}\right), \tag{13}$$

$$\rho_0\omega^2\xi_z = \mathrm{i}kP_T - \frac{\mathrm{i}f_{\mathrm{B}}b_z}{\mu_0} - \frac{b_r}{\mu_0}\frac{\mathrm{d}}{\mathrm{d}r}B_{0z}, \tag{14}$$

$$b_r = \mathrm{i}f_B\xi_r, \tag{15}$$

$$b_\varphi = \mathrm{i}k\left(B_{0z}\xi_\varphi - B_{0\varphi}\xi_z\right) - \frac{\mathrm{d}}{\mathrm{d}r}\left(B_{0\varphi}\xi_r\right), \tag{16}$$

$$b_z = -\frac{\mathrm{i}m}{r}\left(B_{0z}\xi_\varphi - B_{0\varphi}\xi_z\right) - \frac{1}{r}\frac{\mathrm{d}}{\mathrm{d}r}\left(rB_{0z}\xi_r\right), \tag{17}$$

$$p = -\gamma p_0\left(\frac{1}{r}\frac{\mathrm{d}}{\mathrm{d}r}(r\xi_r) + \frac{im}{r}\xi_\varphi + ik\xi_z\right). \tag{18}$$

From the above equations, the dominant Alfvén perturbations are described by Equations (13) & (16). Note, that the perturbations are coupled to the other wave modes, and one may recover the torsional Alfvén wave only if the conditions $m = 0$ and $\mathbf{B}_{0\varphi} = 0$ (i.e. no equilibrium twist) are concurrently satisfied. Straightforward algebra yields the following expressions for the perturbed quantities as functions of the radial component of the displacement

vector (ξ_r) and the Eulerian perturbation of total pressure ($\mathrm{P_T}$):

$$\xi_\varphi = \frac{\mathrm{i}}{D}\left(\frac{m}{r}C_4 - \frac{f_\mathrm{B}B_{0\varphi}}{\mu_0\rho_0}\omega^2\right)\mathrm{P_T} + \tag{19}$$

$$\frac{\mathrm{i}f_\mathrm{B}B_{0\varphi}}{\mu_0\rho_0\omega^2 D}\left(C_1 - \frac{2}{r}C_4\left(\rho_0\omega^2 - \frac{m}{r}\frac{f_\mathrm{B}}{\mu_0}B_{0\varphi}\right)\right)\xi_\mathrm{r}, \tag{20}$$

$$\xi_\mathrm{z} = \frac{\mathrm{i}}{D}\left(kC_4 - \frac{f_\mathrm{B}B_{0\mathrm{z}}}{\mu_0\rho_0}\omega^2\right)\mathrm{P_T} + $$

$$\frac{\mathrm{i}f_\mathrm{B}B_{0\mathrm{z}}}{\mu_0\rho_0\omega^2 D}\left(C_1 + \frac{2}{r}C_4\frac{m}{r}\frac{f_\mathrm{B}}{\mu_0}B_{0\varphi}\right)\xi_\mathrm{r}, \tag{21}$$

$$b_\varphi = -\frac{k}{\rho_0(\omega^2 - \omega_\mathrm{A}^2)}\left(g_\mathrm{B}\mathrm{P_T} - \frac{2f_\mathrm{B}B_{0\varphi}B_{0\mathrm{z}}}{\mu_0 r}\xi_\mathrm{r}\right) - \frac{\mathrm{d}}{\mathrm{d}r}\left(B_{0\varphi}\xi_\mathrm{r}\right), \tag{22}$$

$$b_\mathrm{z} = \frac{m}{r\rho_0(\omega^2 - \omega_\mathrm{A}^2)}\left(g_\mathrm{B}\mathrm{P_T} - \frac{2f_\mathrm{B}B_{0\varphi}B_{0\mathrm{z}}}{\mu_0 r}\xi_\mathrm{r}\right) - \frac{1}{r}\frac{\mathrm{d}}{\mathrm{d}r}\left(rB_{0\mathrm{z}}\xi_\mathrm{r}\right), \tag{23}$$

$$\tag{24}$$

where

$$g_\mathrm{B} = \frac{mB_{0\mathrm{z}}}{r} - kB_{0\varphi}. \tag{25}$$

Note, that the radial perturbed component of the magnetic field b_r is determined directly by Equation (15). In many solar applications it is more practical to use perturbations parallel ($\parallel$) and perpendicular ($\perp$) to magnetic field lines *within* constant magnetic surfaces. These perturbations will represent longitudinal and Alfvén perturbations. For example, in the case of no magnetic twist (i.e. $A = 0$) and for axially symmetric perturbations only (i.e. $m = 0$) the perpendicular perturbations of the magnetic field and velocity within the constant magnetic surfaces would describe the torsional Alfvém waves. In the geometry of the present paper such surfaces are concentric cylinders centred about the z-axis. We introduce the components of the displacement vector and the perturbed magnetic field parallel ($\xi_\parallel$, $b_\parallel$) and perpendicular ($\xi_\perp$, $b_\perp$) to the background equilibrium magnetic field lines within the constant magnetic surfaces given by,

$$\left(\xi_\parallel, b_\parallel\right) = \left(\left(\xi_\varphi, b_\varphi\right)B_{0\varphi} + \left(\xi_\mathrm{z}, b_\mathrm{z}\right)B_{0\mathrm{z}}\right)/B_0, \tag{26}$$

$$\left(\xi_\perp, b_\perp\right) = \left(\left(\xi_\varphi, b_\varphi\right)B_{0\mathrm{z}} - \left(\xi_\mathrm{z}, b_\mathrm{z}\right)B_{0\varphi}\right)/B_0. \tag{27}$$

These components are related to ξ_r and $\mathrm{P_T}$ as,

$$\rho_0(\omega^2 - \omega_\mathrm{C}^2)\xi_\parallel = \frac{\mathrm{i}f_\mathrm{B}}{B_0}\frac{C_\mathrm{S}^2}{C_\mathrm{S}^2 + V_\mathrm{A}^2}\left(\mathrm{P_T} - \frac{2B_{0\varphi}^2}{\mu_0 r}\xi_\mathrm{r}\right), \tag{28}$$

$$\rho_0(\omega^2 - \omega_\mathrm{A}^2)b_\parallel = \frac{g_\mathrm{B}}{B_0}\left(g_\mathrm{B}\mathrm{P_T} - \frac{2f_\mathrm{B}B_{0\varphi}B_{0\mathrm{z}}}{\mu_0 r}\xi_\mathrm{r}\right) - $$

$$\frac{\rho_0(\omega^2 - \omega_\mathrm{A}^2)}{B_0}\left(B_0^2\frac{\mathrm{d}}{\mathrm{d}r}\xi_\mathrm{r} + \frac{B_{0\mathrm{z}}^2\xi_\mathrm{r}}{r} + \xi_\mathrm{r}\frac{\mathrm{d}}{\mathrm{d}r}\frac{B_0^2}{2}\right),$$

$$\rho_0(\omega^2 - \omega_\mathrm{A}^2)\xi_\perp = \frac{\mathrm{i}}{B_0}\left(g_\mathrm{B}\mathrm{P_T} - \frac{2f_\mathrm{B}B_{0\varphi}B_{0\mathrm{z}}}{\mu_0 r}\xi_\mathrm{r}\right),$$

$$\rho_0(\omega^2 - \omega_A^2)b_\perp = -\frac{f_B}{B_0}\left(g_B P_T - \frac{2f_B B_{0\varphi}B_{0z}}{\mu_0 r}\xi_r\right) +$$

$$\frac{\rho_0(\omega^2 - \omega_A^2)}{B_0}\left(\frac{B_{0\varphi}B_{0z}}{r} + B_{0\varphi}\frac{\mathrm{d}}{\mathrm{d}r}B_{0z} - B_{0z}\frac{\mathrm{d}}{\mathrm{d}r}B_{0\varphi}\right)\xi_r.$$
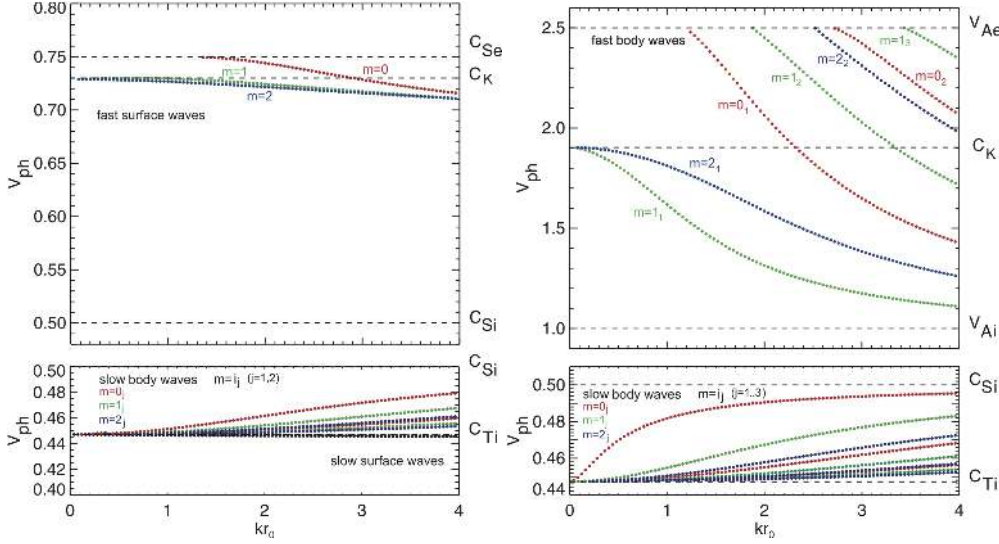

Fig. 11 The dimensionless phase speed (V_{ph}) as function of the dimensionless wavenumber (kr_0) under (a) typical photospheric (i.e $V_{\mathrm{Ai}} > C_{\mathrm{Se}} > C_{\mathrm{Si}} > V_{\mathrm{Ae}}$) and (b) coronal conditions (i.e $V_{\mathrm{Ae}} > V_{\mathrm{Ai}} > C_{\mathrm{Si}} > C_{\mathrm{Se}}$) for an untwisted magnetic flux tube are shown at the (a) left and (b) right panels, respectively. Here (a) $C_{\mathrm{Se}} = 0.75V_{\mathrm{Ai}}$, $V_{\mathrm{Ae}} = 0.25V_{\mathrm{Ai}}$, $C_{\mathrm{Si}} = 0.5V_{\mathrm{Ai}}$ for the photospheric case and (b) $C_{\mathrm{Se}} = 0.25V_{\mathrm{Ai}}$, $V_{\mathrm{Ae}} = 2.5V_{\mathrm{Ai}}$, $C_{\mathrm{Si}} = 0.5V_{\mathrm{Ai}}$ for the solar corona. In the left panel three modes of the fast surface waves that are bounded within $[C_{\mathrm{Si}}, C_{\mathrm{Se}}]$ and the infinite number of the slow body waves bounded within $[C_{\mathrm{Ti}}, C_{\mathrm{Si}}]$ are plotted. The slow kink, sausage, etc. surface waves are very close to each other (just under C_{Ti}). In the right panel sausage (m=0), kink (m=1) and fluting (m=2) modes are shown. The infinite number of the fast body waves are bounded within $[V_{\mathrm{Ai}}, V_{\mathrm{Ae}}]$ and the infinite number of the slow body waves are bounded within $[C_{\mathrm{Ti}}, C_{\mathrm{Si}}]$. $m = i_j$, where the i refers to the mode (sausage, kink, etc.) and j refers to the j-th branch of the zeroes of eigenfunctions in the radial direction. Only three branches of each mode of the infinitely many slow and fast body waves are plotted.

These governing equations, in various alternative formats, were derived previously in various contexts by e.g. Hain & Lüst (1958), Goedbloed (1971), Appert et al. (1974), Goossens (1991), Sakurai et al. (1991) and Erdélyi & Fedun (2006, 2007, 2010).

5.3 Derivation of the General Dispersion Equation

Applying the boundary conditions to the inside and outside solutions of the governing equations yields the required general dispersion relation that will determine the existing wave modes of the system. The continuity condition for the radial component of the displacement,

$$\xi_{\mathrm{ir}}|_{r=r_0} = \xi_{\mathrm{er}}|_{r=r_0},$$

and the continuity of pressure,

$$P_{Ti} - \frac{B_{0i\varphi}^2}{\mu_0 r_0} \xi_{ir}\bigg|_{r=r_0} = P_{Te}|_{r=r_0}$$

provide the desired dispersion relation:

$$D_e \frac{r_0}{m_{0e}} \frac{K_m(m_{0e}r_0)}{K'_m(m_{0e}r_0)} = -\frac{A^2 r_0^2}{\mu_0^2} + D_i r_0^2 \frac{(1-\alpha^2)}{m(1-\alpha) + 2x_0 \frac{M'(a,b,x_0)}{M(a,b,x_0)}}. \tag{29}$$

The dash denotes the derivative of the Kummer's function evaluated at $x = x_0$, where

$$x_0 = \frac{n}{k} E^{1/2} k_\alpha^2 r_0^2. \tag{30}$$

Equation (29) is the *general dispersion equation* for linear MHD waves in a magnetically uniformly twisted compressible flux tube embedded in a compressible and uniform straight magnetic environment. To the best of our knowledge, it is not possible to solve analytically Equation (29) in general terms. However, at least certain checks can be carried out, e.g. applying the incompressible limit should recover the dispersion relation of Bennett et al. (1999) or Erdélyi & Fedun (2006). Another limiting case is $B_{0\varphi} \to 0$ where the well known dispersion relation Equations (8a, b) of Edwin & Roberts (1983) must be recovered. These particular cases of analytical checks reassure us that the derivations are consistent. Although we would prefer further analytical insight, such approach seems to be limited by the lack of existing suitable asymptotic expansions for Kummer functions $M(a,b,x_0)$ and $M'(a,b,x_0)$. We shall here only recall a typical graphical solution of the dispersion relation, revealing all the linear MHD modes.

In Figure 11 the results of calculations of the dispersion curves derived from Equation (29) are presented. One can observe here the very rich structure of linear MHD modes. Note, the Alfvén waves are just a single line, as all the modes have the same phase speed. The modes can often only be distinguished from other magneto-acoustic (e.g. kink) modes, if one carefully determines the polarisation. This can be rather hard, given the currently available observational tools.

6 Concluding remarks

There are at least three fundamental questions that must be resolved in order to understand the heating of the solar (and stellar) atmosphere: Where is the energy generated? How does the generated energy propagate from the energy reservoir to the solar atmosphere, spanning from the warm chromosphere to the corona? How does the transported energy efficiently dissipate in the solar atmosphere in order to maintain its multimillion-Kelvin temperature? There are numerous examples of slow and fast MHD waves observed in the solar atmosphere. However, their energy density does not seem sufficient for coronal heating or powering the solar wind. On the other hand, among MHD wave theorists, Alfvén waves still remain the "Holy Grail" of coronal heating, solar wind acceleration and solar magneto-seismology (Banerjee et al. 2007).

The applicability of MHD wave research to magneto-seismology is a relatively recent development. The main idea here is to determine information about the MHD waveguide in which the waves propagate. This is analogous to the techniques of seismology, a popular

method of investigating the sub-surface structure of the Earth. The difference here is that in a magnetised plasma there is a plentiful abundance of waves in existence, offering us various aspects of seismology. The frequency (or period) measurements of MHD waves are often used to determine density and magnetic stratification, both in the longitudinal and transversal directions of the waveguide. More recently, however, studies of the spatial distribution of waves and their intrinsic characteristics have been suggested, offering an independent method to determine diagnostic information about the waveguide (Erdélyi & Verth 2007; Verth et al. 2007). Magneto-seismology has a novel application to the reconstruction of MHD waveguides. This is perhaps an even more important aspect compared to the others. The idea here is that by studying the properties of MHD waves and oscillations, their distribution in the waveguide (assuming here an adequate spatial and temporal resolution) may help construct detailed magnetic surface topology. The idea has been outlined in a recent paper by Verth et al. (2010) and Fedun et al. (2011b).

There have been some suggestions that transversal waves may be considered Alfvénic in nature providing that they are incompressible, exhibit no intensity fluctuations and display periodic displacements with the magnetic tension as the restoring force (Goossens et al. 2009). The terminology of Alfvénic is, however, not entirely clear as such waves do not normally exist as an eigenvalue of the linear MHD equations in structured plasmas: on the other hand many magnetic oscillating structures in the corona and below can not be described by pure linear MHD eigenmodes. Given the ambiguity, it may be better to refer to these waves as transversal (Jess et al. 2012). Further, refined observations, with the use of e.g. spectro-polarimetric measurements, may be able to clarify the wave mode identity with greater accuracy.

According to Cirtain et al. (2007) and De Pontieu et al. (2007), signatures of Alfvén waves were observed with the use of the XRT and SOT instruments, respectively. Because these jets are increases in local density, if their length is short relative to the wavelength of Alfvén perturbations, they can slide along magnetic field lines, and act as test particles (see the yellow-red blob in Fig. 9b) in the plasma that has almost no resistivity, just like bobsleds would run and slide along a prebuilt track. However, these observations also raise concerns about the applicability of the classical concept of a magnetic flux tube in the very dynamic solar atmosphere, where these sliding jets were captured. In a classical magnetic flux tube, propagating Alfvén waves along the tube would cause torsional oscillations (Fig. 9a). In this scenario, the only observational signature of Alfvén waves would be spectral line broadening, as observed by Jess et al. (2009). On the other hand, if these classical flux tubes did indeed exist, then the observations of De Pontieu et al. (2007) would be interpreted as kink waves (i.e. waves that displace the axis of symmetry of the flux tube like an S-shape). More detailed observations are needed, so that a full three-dimensional picture of wave propagation could emerge.

Numerical simulations of a two-dimensional stratified VAL-atmosphere model (Vernazza et al. 1981), embedded in a horizontal magnetic field to mimic solar prominences and driven by global photospheric motions, will also result into observational signatures very similar to those reported by Okamoto et al. (2007), and in Figure 2 and the online movie S1 of Erdélyi & Fedun (2007). In particular, note the similarity between the time-distance plot (Fig. 2a) of the illustrative forward modelling simulations in Erdélyi & Fedun (2007) and Figure 3 of Okamoto et al. (2007). However, in the case of this numerical forward modelling experiment the oscillations found are clearly not Alfvénic, but are rather transversal kink oscillations.

It is worth mentioning what may be some key directions where MHD, in particular, Alfvén wave research may develop. Among the many possibilities is the development of

Alfvén (and in parallel other MHD) wave theory in dynamic plasma. Observations indicate that waveguides change, often considerably, during the time that the oscillations reported are guided by them (Aschwanden & Terradas 2008). As long as the characteristic time scale of the changes in the background plasma are small or comparable to the time scales of waves crossing the structure, some initial theoretical progress has already been made (Morton & Erdélyi 2009, 2010; Morton et al. 2010, 2011; Ruderman 2011a,b). It is a real challenge to develop wave theory in dynamic plasmas. Another fascinating aspect of developments will be the advancement of (non)linear Alfvén and magneto-acoustic waves where the geometry and structuring of the waveguide is more complex but more realistic. Significant technological improvements associated in High Performance Computing will allow detailed MHD wave studies of the coupled solar interior-atmosphere system as a whole. Such studies will shed ample light into the true nature of Alfvén and other MHD wave dynamics and heating (Bogdan et al. 2003; Carlsson & Bogdan 2006; Erdélyi et al. 2007; Fedun et al. 2009; Khomenko et al. 2008; Fedun et al. 2011a).

Last, but by no means least, we will provide some observational goals that will hopefully assist the detection, disambiguation, and study of solar oscillations. High-cadence imagers, such as the ROSA (Jess et al. 2010) instrument, will need to be employed with high spatial, temporal, *and* spectral resolution facilities, such as the IBIS (Cavallini 2006) and CRISP (Scharmer et al. 2008) two-dimensional spectro-polarimeters. Simultaneous observations between the ground-based instruments and state-of-the-art space-borne facilities such as SDO, and the planned IRIS (Interface Region Imaging Spectrograph) can provide the necessary intensity, magnetic-field, and Doppler signals required to unveil the specific wave modes as they travel through the solar atmosphere. The Helioseismic and Magnetic Imager (HMI) on SDO provides dopplegrams, continuum filtergrams, line-of-sight and vector magnetograms at the solar surface, thus allowing the sites of photospheric oscillations to be identified (albeit at a lower spatial resolution). The Atmospheric Imaging Assembly (AIA) provides the coronal magnetic field configuration, which can be compared to that obtained by HMI. IRIS in particular will obtain high spatial (250 km) and temporal resolution (1 sec) spectra and images in ultraviolet wavelengths, focusing on the upper chromosphere and transition region. The combination of simultaneous imaging and spectroscopy provided by IRIS will allow us to disentangle the velocity and intensity signal of torsional, kink and sausage wave modes as they travel through the complex interface between the photosphere and the corona. High resolution limb spectro-polarimetry of chromospheric structures such as spicules and prominences remains a major challenge. The low photon statistics at the solar limb, limit the use of Adaptive Optics and the number of photons required for the measurement of accurate Stokes profiles. These difficulties will be overcome with the upcoming Advanced Technology Solar Telescope (Keil et al. 2010), with a 4 m primary mirror, will allow structures in the Sun's atmosphere to be examined on unprecedented spatial scales of ≈ 20 km.

References

N. Akinari ApJ **660** 1660 (2007)

G. Alazraki, P. Couturier A&A **13** 380 (1971)

H. Alfvén Nature **150** 405 (1942)

H. Alfvén MNRAS **107** 211 (1947)

K. Appert, R. Gruber, J. Vaclavik Phys. Fluids **17** 1471 (1974)

I. Arregui, R. Oliver, J.L. Ballester Living Rev. Solar Phys. **9** lrsp-2012-2 (2012)

M.J. Aschwanden, L. Fletcher, C.J. Schrijver, D. Alexander ApJ **520** 880 (1999)

M.J. Aschwanden, J. Terradas ApJ **686** L127 (2008)

G. Aulanier, E. Pariat, P. Démoulin, C.R. Devore Solar Physics **238** 347 (2006)

D. Banerjee, R. Erdélyi, R. Oliver, E. OShea Solar Physics 246 136 (2007)

T.L. Bogdan, M. Carlsson, V.H. Hansteen et al. ApJ **599** 626 (2003)

J.W. Belcher JApJ **168** 509 (1971)

J.W. Belcher, L. Davis J. Geophys. Res. **76** 3534 (1971)

K. Bennett, B. Roberts, U., Narain Solar Phys. **185** 41 (1999)

P. Boerner, C. Edwards, J. Lemen, et al. Solar Phys. **316** (2011)

J.A. Bonet, I. Márquez, J. Sánchez Almeida, et al. ApJ **687** L131 (2008)

D.S. Bloomfield, R.T.J. McAteer, M. Mathioudakis et al. ApJ **604** 936 (2004)

R. Bruno, V. Carbone Living Rev. Solar Phys. **2** lrsp-2005-4 (2005)

M. Carlsson & T.J. Bogdan Royal Society of London Philosophical Transactions Series A **364** 395 (2006)

M. Carlsson, R.F. Stein ApJ **481** 500 (1997)

G. Cauzzi, K. Reardon, R.J. Rutten, A. Tritschler, H. Uitenbroek A&A **503** 577 (2009)

F. Cavallini Solar Phys. **236**, 415 (2006)

J. Chae, U. Schühle, P. Lemaire ApJ **505** 957 (1998)

C-C. Cheng, G.A. Doschek, U. Feldman ApJ **227** 1037 (1979)

J.W. Cirtain, L. Golub, L. Lundquist, et al. Science **318** 1580 (2007)

P.J. Coleman Jr. P&SS **15** 953 (1967)

S.R. Cranmer, A.A. Ballegooigen ApJS **156** 265 (2005)

T. Darnell, S. Tomczyk, G. Card, et al. AGU Fall Meeting Abstracts, **505** (2003)

J.M. Davila ApJ, **317** 514 (2003)

I. De Moortel, A.W. Hood, C.L. Gerrard, & S.J. Brooks A&A **425** 741 (2004)

L. Del Zanna, M. Velli, P. Londrillo A&A **367** 705 (2001)

B. De Pontieu, R. Erdélyi, S.P. James Nature **430** 536 (2004)

B. De Pontieu, S.W. McIntosh, M. Carlsson, et al. Science **318** 1574 (2007)

G.A. Doschek, J.D. Bohlin, U. Feldman ApJ **205** L177 (1976)

P.M. Edwin, B. Roberts Solar Phys. **76** 239 (1982)

P.M. Edwin, B. Roberts Solar Phys. **88** 179 (1983)

G. Einaudi, M. Velli, H. Politano, A. Pouquet ApJ **457** L113 (1996)

A.G. Emslie, M.E. Machado, Sol. Phys. **64** 129 (1979)

A.G. Emslie, P.A. Sturrock, Solar Physics **80** 99 (1982)

R. Erdélyi Royal Society of London Philosophical Transactions Series A **364** 351 (2006a)

R. Erdélyi Proceedings of SOHO 18/GONG 2006/HELAS I, Beyond the spherical Sun, eds. K. Fletcher, K. & M. Thompson, **ESA SP-624** 15 (2006b)

R. Erdélyi, J.G. Doyle, M.E. Perez, K. Wilhelm A&A **337** 287 (1998)

R. Erdélyi, V. Fedun Solar Phys. **238** 41 (2006)

R. Erdélyi, V. Fedun Solar Phys. **246** 101 (2007)

R. Erdélyi, V. Fedun Science **318** 1572 (2007)

R. Erdélyi, V. Fedun Solar Phys. **263** 63 (2010)

R. Erdélyi, M. Goossens, Astron. Astrophys. **294**, 575 (1995)

R. Erdélyi, C. Malins, G. Tóth, B. De Pontieu A&A **467** 1299 (2007)

R. Erdélyi, G. Verth A&A **462** 743 (2007)

V. Fedun, R. Erdélyi, S. Shelyag, S. Solar Phys., **258** 219 (2009)

V. Fedun, S. Shelyag, R. Erdélyi ApJ **727** 17 (2011a)

V. Fedun, G. Verth, D.B. Jess, R. Erdélyi ApJ **740** L46 (2011b)

L. Fletcher, H.S. Hudson ApJ **675** 1645 (2008)

M. Fujimoto, I. Shinohara, H. Kojima Space Sci. Rev. **160** 123 (2011)

D. Fujimura, S. Tsuneta ApJ **702** 1443 (2009)

W. Gekelman JGR **104** 14417 (1999)

M.K. Georgoulis, M. Velli, G. Einaudi ApJ **497** 957 (1998)

J.P. Goedbloed Physica D **53** 412 (1971)

J.P. Goedbloed, G. Halberstadt A&A **286** 275 (1994)

D.O. Gomez Fund. Cosmic Phys. **14** 131 (1990)

M. Goossens Advances in Solar System Magnetohydrodynamics, Cambridge University Press. CUP (1991)

M. Goossens, R. Erdélyi, M.S. Ruderman Space Sci. Rev. **158**, 289 (2011)

M. Goossens, J. Terradas, J. Andries, I. Arregui & J.L. Ballester A&A **503** 213 (2009)

K. Hain, R. Lüst Z. Naturforsch **13a** 936 (1958)

S.S. Hasan, W. Kalkofen ApJ **519** 899 (1999)

J.-S. He, C.-Y. Tu, E. Marsch, L.-J. Guo, S. Yao, H. Tian A&A **497** 525 (2009)

M. Heinemann, S. Olbert JGR **85** 1311 (1980)

J. Heyvaerts, E.R. Priest A&A **117** 220 (1983)

J.V. Hollweg, in (eds.) P. Ulmschneider, E.R Priest, R. Rosner Mechanisms of Chromospheric and Coronal Heating, Springer-Verlag, Berlin. 423 (1991)

J.V. Hollweg, Solar Phys. **70** 25 (1981)

J.V. Hollweg, S. Jackson, D. Galloway Solar Phys. **75** 35 (1982)

J.V. Hollweg, G. Yang JGR **93** 5423 (1988)

C.L. Hyder Z. Astrophys. **63** 78 (1966)

J.A. Ionson, Astrophys. J. **226**, 650 (1978)

D.B. Jess, M. Mathioudakis, D.J. Christian, et al. Solar Phys. **261** 363 (2010)

D.B. Jess, M. Mathioudakis, R. Erdélyi, et al. Science **323** 1582 (2009)

D.B. Jess, D.J. Pascoe, D.J. Christian, et al. ApJ **744** L5 (2012)

W. Kalkofen ApJ **486** L145 (1997)

Keil, S. L., Rimmele, T. R., Wagner, J., & ATST team, Astronomische Nachrichten, **331**, 609 (2010)

A. Keiling Space Sci. Rev. **142** 73 (2009)

E. Khomenko, M. Collados, T. Felipe Solar Phys. **251** 589 (2008)

J.A. Klimchuk Solar Physics **234** 41 (2006)

J.A. Klimchuk, S.K. Antiochos, D. Norton ApJ **542** 504 (2000)

M. Kuperus, J.A. Ionson, D.S. Spicer Ann. Rev. Astron. Astrophys. **19** 7 (1981)

H. Lin, M.J, Penn, S. Tomczyk ApJ **541** L83 (2000)

M.E. Machado, A.G. Emslie, J.C. Brown Solar Physics **58** 363 (1978)

F. Malara, M. Velli Phys. Plasmas **3** 4427 (1996)

F. Malara, P. Petkaki, P. Veltri ApJ **533** 523 (2000)

F. Malara, F. Primavera, P. Veltri Phys. Plasmas **7** 2866 (2000a)

E. Marsch Living Rev. Solar Phys. **2** lrsp-2006-1 (2006)

J. Martinez-Sykora, V. Hansteen, B. DePontieu, M. Carlsson ApJ **701** 1569 (2009)

W.H. Matthaeus, G.P. Zank, S. Oughton, D.J. Mullan, P. Dmitruk ApJ **523** L93 (1999)

W.H. Matthaeus, M. Velli Space Sci. Rev. **160** 145 (2011)

R.T.J. McAteer, P.T. Gallagher, D.R. Williams et al. ApJ **587** 806 (2003)

J.A. McLaughlin, L. Ofman ApJ **682** 1338 (2008)

K.G McClements, R.A. Harrison, D. Alexander Solar Physics **131** 41 (1991)

S.W. McIntosh, B. DePontieu, T.D. Tarbell ApJ **673** L219 (2008)

S.W. McIntosh, B. DePontieu, M. Carlsson, V. Hansteen, P. Boerner, M. Goossens Nature **475** 477 (2011)

G.E. Moreton, H.E. Ramsey PASP **72** 357 (1960)

R.J. Morton, R. Erdélyi ApJ **707** 750 (2009)

R.J. Morton, R. Erdélyi A&A **519** 23 (2010)

R.J. Morton, A.W. Hood, R. Erdélyi A&A **512** 23 (2010)

R.J. Morton, M.S. Ruderman, R. Erdélyi A&A **534** 27 (2011)

Z.E. Musielak, P. Ulmschneider A&A **406** 725 (2003)

V.M. Nakariakov, L. Ofman, E.E. Deluca, B. Roberts, J.M. Davila Science **285** 862 (1999)

V.M. Nakariakov, E. Verwichte LRSP **2** 3 (2005)

L. Ofman, M.J. Aschwanden ApJ **576** L153 (2002)

L. Ofman, J.M. Davila, R. S. Steinolfson ApJ **421** 360 (1994)

L. Ofman, J.M. Davila, R. S. Steinolfson ApJ **444** 371 (1995)

L. Ofman, J.M. Davila JGR **100** 23427 (1995)

L. Ofman, J.M. Davila JGR **103** 23677 (1998)

L. Ofman SSRv **120** 67 (2005)

L. Ofman, A.F. Viñas JGR **112** A06104 (2007)

L. Ofman, T.J. Wang A&A **482** L9 (2008)

L. Ofman SSRv **149** 153 (2009)

L. Ofman ApJ **694** 502 (2009a)

L. Ofman Living Rev. Solar Phys. **7** lrsp-2010-4 (2010)

L. Ofman JGR **115** A04108 (2010a)

T.J. Okamoto, S. Tsuneta, T.E. Berger, et al. Science **318** 1577 (2007)

D.E. Osterbrock ApJ **134** 347 (1961)

E.N. Parker, ApJ **330** 474 (1988)

S. Poedts, M. Goossens, W. Kerner Solar Physics **123** 83 (1989)

S. Poedts, M. Goossens, W. Kerner ApJ **360** 279 (1990)

M.A. Raadu, Solar Physics **22** 425 (1972)

A.F. Rappazzo, M. Velli, G. Einaudi, R.B. Dahlburg, ApJ **677** 1348 (2008)

B. Pintér, R. Erdélyi Space Sci Rev. **158** 471 (2011)

E.R. Priest, C.J. Schrijver Solar Phys. **190** 1 (1999)

N.-E. Raouafi & Solanki A&A **445** 735 (2006)

B. Roberts Solar Phys. **61** 23 (1979)

B. Roberts, Solar Physics **69** 39 (1981)

B. Roberts, Solar Physics **193** 139 (2000)

M.S. Ruderman, ApJ **521** 851 (1999)

M.S. Ruderman, Solar Physics **271** 41 (2011a)

M.S. Ruderman, A&A **534** A78 (2011b)

M.S. Ruderman, D. Berghmans, M. Goossens, S. Poedts A&A **320** 305 (1997)

M.S. Ruderman, B. Roberts ApJ **577**, 475 (2002)

T. Sakurai, M. Goossens, J.V. Hollweg Solar Phys. **133** 227 (1991)

J. Sánchez Almeida, J.A. Bonet, B. Viticchié, & D. Del Moro ApJ **715** L26 (2010)

Scharmer, G. B., Narayan, G., Hillberg, T., et al., ApJ, **689**, L69 (2008)

J.M. Schmidt, L. Ofman ApJ **739** 75 (2011)

J. Scudder ApJ **398** 299 (1993a)

J. Scudder ApJ **398** 319 (1993b)

M. Selwa, L. Ofman ApJ **714** 170 (2010)

M. Selwa, L. Ofman, S.K. Solanki ApJ **726** 42 (2011a)

M. Selwa, S.K. Solanki, L. Ofman ApJ **728** 87 (2011b)

S. Shelyag, P.H. Keys, M. Mathioudakis, F.P. Keenan A&A **526** A5 (2011)

K. Shibata, Y. Ishido, W.L. Acton et al. PASJ **44** L173 (1992)

R.F. Stein, A. Nordlund ApJ **499** 914 (1998)

R. S. Steinolfson, J. M. Davila ApJ **415** 354 (1993)

A.C. Sterling, & J.V. Hollweg ApJ **327** 950 (1988)

J.J. Sudol, J.W. Harvey ApJ **635** 647 (2005)

T.K. Suzuki, S. Inutsuka ApJ **632** L49 (2005)

Y. Taroyan, R. Erdélyi Space Sci Rev. **149** 229 (2009)

J.H. Thomas, D.C.H. Stanchfield II ApJ **537** 1086 (2000)

A. Title Advances in Space Research **4** 67 (1984)

S. Tomczyk, S.W. McIntosh, S.L. Keil, et al. Science **317** 1192 (2007)

S. Tomczyk, S.W. McIntosh ApJ **697** 1384 (2009)

D. Tripathi, H. Isobe, R. Jain SSRv **149** 283 (2009)

S. Tsuneta, K. Ichimoto, Y. Katsukawa, et al. Solar Phys., **249** 167 (2008)

B.T. Tsurutani, C.M. Ho Rev. Geophys, **37** 517 (1999)

A.A. van Ballegooijen, M. Asgari-Targhi, S.R. Cranmer, E.E. DeLuca ApJ **736** 3 (2011)

T. Van Doorsselaere, V. Nakariakov, E. Verwichte ApJ **676** L73 (2008)

M. van Noort, L.H.M. Rouppe van der Voort, M.G. Lofdahl Solar Physics **228** 191 (2005)

M. Velli, R. Grappin, A. Magneney PRL **63** 1807 (1989)

M. Velli A&A **270** 304 (1993)

M. Velli, P. Liewer SSR **87** 339 (1999)

M. Velli Plasma Phys. Control Fusion **45** A205 (2003)

A. Verdini, M. Velli, E. Buchlin ApJ **700** L39 (2009)

J.E. Vernazza, E.H. Avrett, R. Loeser ApJS **45** 635 (1981)

G. Verth, Van Doorsselaere, T., R. Erdélyi, M. Goossens A&A **475** 341 (2007)

G. Verth, R. Erdélyi, M. Goossens ApJ **714** 1637 (2010)

G. Vigeesh, V. Fedun, S.S. Hasan, R. Erdélyi 2011arXiv1109.6471V

J. Vranjes, S. Poedts, B. P. Pandey, & B. de Pontieu, A&A **478** 553 (2008)

B. Vršnak, A.M. Veronig, J.K. Thalmann, T. Źic A&A **471** 295 (2007)

T.W.J. Unti, M. Neugebauer PhFl **11** 563 (1968)

S. Wedemeyer-Bohm, L. Rouppe van der Voort ApJ **507** L9 (2009)

T.V. Zaqarashvili A&A **399** L15 (2003)

T. V. Zaqarashvili, R. Erdélyi Space Sci Rev. **149** 355 (2009)

Y.Z. Zhang, K. Shibata, J.X. Wang, X.J. Mao, T. Matsumoto, Y. Liu, J.T. Su ApJ **750** 16 (2012)

J. B. Zirker Solar Physics **148** 43 (1993)